2020HGW

Properties of an Unusually Bright Type II Supernova

Masters Thesis

Written by *Maja Skafsgaard*

October 29, 2022

Supervised by

Charlotte Angus & Christa Gall

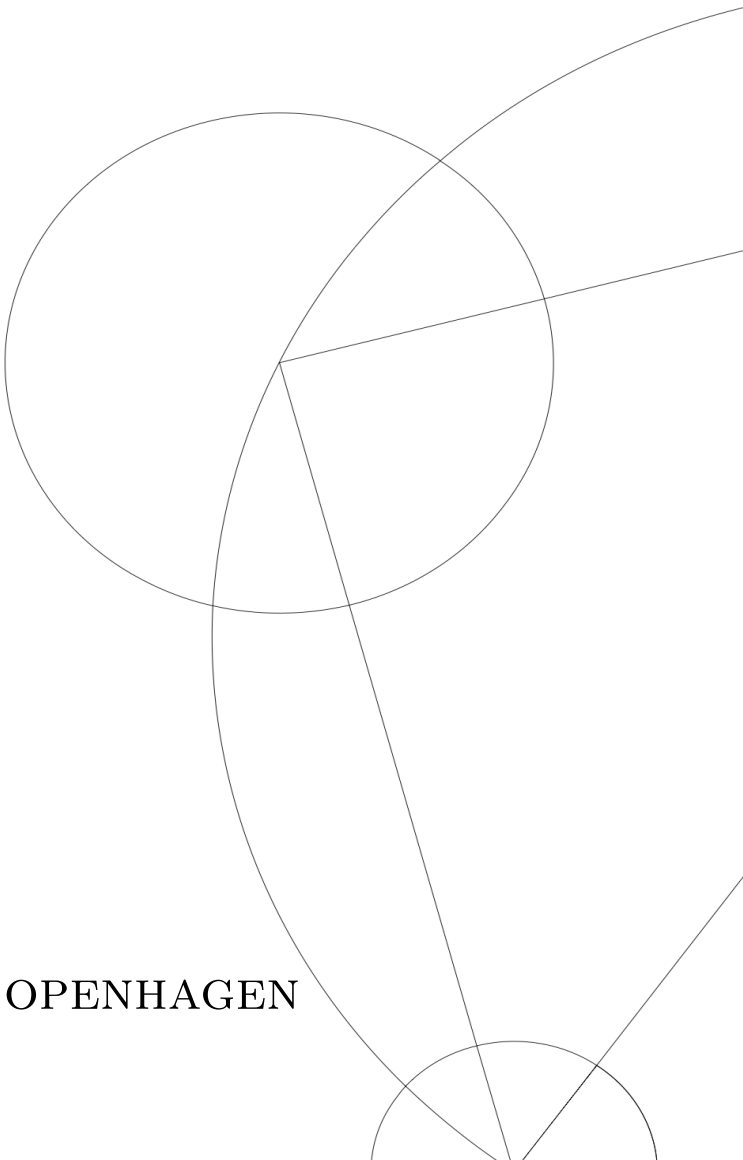

University of Copenhagen

UNIVERSITY OF COPENHAGEN

Name of Institute:	The Niels Bohr Institute
Name of Department:	Dark Cosmology Centre
Author(s):	Maja Skafsgaard
Email:	vwk284@alumni.ku.dk
Title and subtitle:	2020hgw - Properties of an Unusually Bright Type II Supernova
Supervisor(s):	Charlotte Angus & Christa Gall
Handed in:	31.10.2022
Defended:	28.11.2022

Name _____

Signature _____

Date _____

Abstract

In this thesis I present photometric and spectroscopic analysis of the atypical Type II Supernova, 2020hgw, and compare its properties to a sample population of Type II SNe. 2020hgw appears remarkably bright and seems to exhibit a very short plateau in its r-band light curve. I find the peak absolute r-band magnitude to be -18.69 ± 0.065 and through analysis of the light curve I find the plateau duration to be $Pd = 31.70 \pm 0.64$ days and the duration of the optically thick phase to be $OPTd = 59.79 \pm 0.44$ days. I also measure the decline rate from the peak to the beginning of the plateau, $s_1 = 0.024 \pm 0.006$, and the decline rate of the plateau, $s_2 = 0.011 \pm 0.005$. I statistically and visually inspect whether the light curve is best fitted with or without a plateau, and find the best fit for the r-band to include a plateau. From fitting the H_α P-Cygni profiles at four different epochs, I find the expansion velocities from the absorption and emission lines and the ratio of absorption to emission, a/e. At a comparable epoch to the comparison sample, I measure the H_α absorption velocity to be $H_\alpha velocity = 4314.11 \pm 12.03 km\,s^{-1}$ and the ratio to be $a/e = 0.4321 \pm 0.0003$. I measure the total radiated energy to be $1.559 \pm 0.004 \times 10^{44} erg\,s^{-1}$. I find that for most of the parameters, 2020hgw lies within the general scatter of the whole Type II SN sample, however, it is atypical for a bright Type II SN with much lower s_1, s_2 and $H_\alpha velocity$ and relatively higher a/e, but comparable Pd and $OPTd$. I discuss some of the implications of these results. Whether 2020hgw is a typical example of a 'short plateau SN' or an exceptional case is unclear.

Contents

1 Introduction **4**

1.1 Supernovae 4

1.2 Core Collapse 4

1.3 Type II Supernovae 5

1.3.1 The Plateau 7

1.4 The P-Cygni Profile 8

1.5 2020hgw: At First Glance 9

1.6 Why is 2020hgw Interesting? 10

2 The Data **12**

2.1 2020hgw: Photometric Data 12

2.1.1 ZTF 12

2.1.2 YSE 12

2.1.3 ATLAS 13

2.1.4 SWIFT 13

2.2 Photometric Data Utilised 15

2.3 2020hgw: Spectroscopic Data 17

2.4 The Comparison Samples 20

2.4.1 Anderson et al. 2014 20

2.4.2 Gutiérrez et al. 2014 20

3 Methods **21**

3.1 Superbol 21

3.2 Olivares and the Curve 23

3.3 Anderson et al. 2014 25

3.4 The Fitting Process and Other Side Quests 27

3.4.1 Fitting the Light Curve 27

3.4.2 Fitting s_1 and s_2 28

3.4.3 Fitting the H_α lines 29

4 Results **30**

4.1 The Plateau 30

4.2 Fits to the Light Curve 32
4.3 Finding t_{tran} and t_{end} 34
4.4 The Fitting of s_1 and s_2 35
4.5 Anderson et. al 2014 and Their SNe 37
4.6 Spectra and Spectral Fits 39
4.7 Gutiérrez et al. 2014 and their SNe 46
4.8 The Bolometric Lightcurve 50

5 Discussion **51**

6 Conclusion **56**

7 Acknowledgments **57**

References **57**

1 Introduction

1.1 Supernovae

Compared to the duration of a star's life, the Supernova(SN) which occurs at the end of a stars life and marking its explosive death, is relatively short. This means that the window for observing them is quite short, and only a small fraction of stars even have the potential to become a SN as it is only massive stars($M > 8 - 10M_{\odot}$) and white dwarves in binary systems that end their life this way.[1]
In the Milky Way only about three stars per century erupt in SN explosions[1] making it ever more important to survey outside the Milky Way. Fortunately, transient astronomy is a rapidly changing field and professional astronomers are able to utilise numerous large, wide field sky surveys making way for the discovery of hundreds of new transients every night.

At an ever increasing rate, many extreme, exotic and strange events are revealed and new and unheard of classes of SNe are unearthed urging a redefinition of what is 'normal'.
In this thesis I will focus upon the properties of one of these events: 2020hgw, an unusual core collapse SN.

1.2 Core Collapse

Throughout their lives massive stars get hot enough to fuse elements through the C-N-O-cycle (Carbon-Nitrogen-Oxygen), where Hydrogen is fused into Helium through at catalytic cycle[2]. As the star is depleted of Hydrogen, it starts fusing heavier elements in an onion-like structure with Helium-fusion in the outermost shell, and Carbon, Neon, Oxygen and Silicon in the successive shells. Silicon fusion however, produces Iron and because Iron fusion requires energy instead of producing energy, Iron therefore starts to build up at the centre rather than contributing to the energy output.

Once the mass of the Iron core reaches the Chandrasekhar limit of $M_{core} \sim 1.44M_{\odot}$, we have come to the stage where most massive stars end their lives: as a core collapse SN. The atoms in the Iron core become relativistic and electron degeneracy pressure is no longer enough against the pull of gravity. The Iron core that has been

growing to become about the size of the Earth collapses to roughly 10-30 km in size, with all of this taking about 1/4 of a second.[3]
As the star compresses to about 10 km at enormous speed, it overshoots and therefore rebounds. This rebound drives a shock wave into the shells of stellar material surrounding the core, all of which were being pulled into the star by gravity. The shock wave is however damped by the collision with the infalling material and is stalled.

During this process, all of the protons and electrons in the core start to combine to form neutrons: the ingredients of a neutron star. For each neutron produced, an electron neutrino is also produced and emitted, carrying away more energy from the collapsing star.
The core rebounds again sending out this immense flow of neutrinos that propagate out through the material, boosting the previously stalled shock wave: the shock waves and the neutrino wave now combine in power and erupt in the actual SN explosion.[4] This explosion is such an energetic one that it very quickly brightens to billions of solar luminosities, and often SNe outshine their host galaxies.

1.3 Type II Supernovae

Spectroscopically SNe are classified into two groups and several subgroups; Type I or II, and then Ia, Ib/c, II-Plateau(IIP), II-Linear(IIL), II-narrow(IIn) or IIb. Ia are the only SNe that are caused by runaway thermal fusion, whereas almost all the other types are core collapse SNe.

As can be seen in Figure 1, the first step in classification is to find out whether there is Hydrogen in the spectrum: Type I SNe have no Hydrogen, but instead either silicon or helium lines, whereas Type II have Hydrogen lines. For Type IIb these are weak and they later change to look like a Ib. For Type IIn the emission lines have a very broad base, and intermediate middle, and the centre is a very narrow spike of emission, hence the 'n' in IIn. For Type IIs these emission and absorption lines are intermediate and broad, indicating expansion velocities anywhere from some hundreds up to many thousands of kilometres per second.
From current knowledge, Type II SNe are believed to come from the collapse of stars of initial masses at $8 - 18 M_{\odot}$.[6] This means they are fairly large stars, but not so

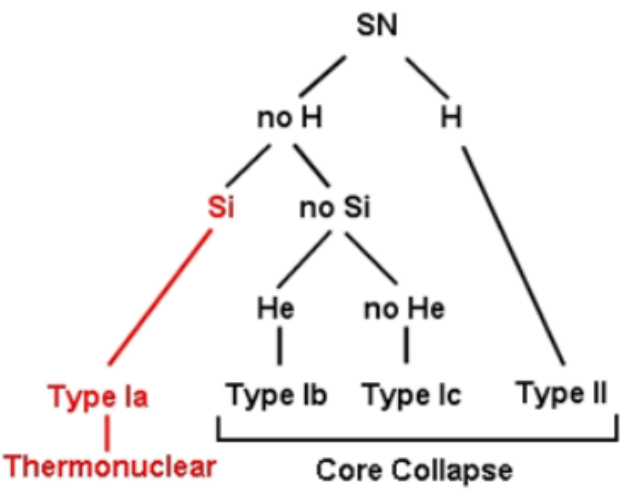

Figure 1: Supernova classification tree.[5]

massive that they have lost all of their Hydrogen to winds when they explode.

Until recently it was believed that there was an inherent difference between type IIPs and IILs as they were distinguished based upon their light curves. For IILs, the light curve decreases linearly over time from peak luminosity to the radioactive tail, whereas IIPs reach a plateau during the decline. The difference between the two is shown in Figure 2.

Furthermore, we know from pre-explosion images that the progenitors of Type IIPs are red supergiants(RSG)[7], whereas the progenitors of Type IILs remain unknown. Despite their seemingly clear difference and previous theories that IIPs and IIL are inherently different, they should arise from a continuous distribution of progenitor stars given that the division of the two types is arbitrarily based on their photospheric properties and not spectroscopic properties. Additionally, the larger, and still growing, samples of type II SNe are showing a more continuous distribution of properties between the two classes. This would dispute the theories that they are inherently different, and maybe there is no strong physical distinction between their progenitors.

Nonetheless, the shortest plateaus observed thus far are no shorter than approximately 50 days[8], when in theory we should observe many shorter plateaus if they were from the same population.

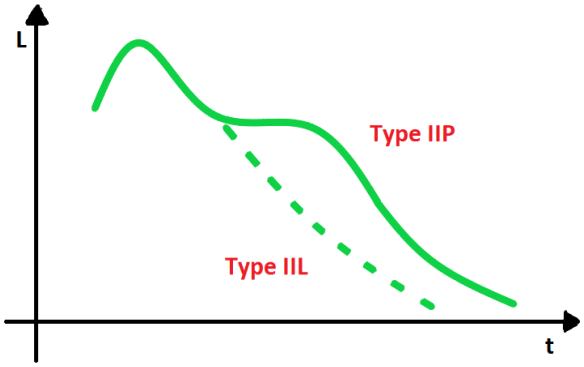

Figure 2: Light curves of Type IIP vs Type IIL SNe.

1.3.1 The Plateau

Most of the observed Type II SNe are IIPs[9], and the plateau of the Type IIP's light curve marks the stage where the photosphere of the SN has cooled to 5000-7000 K. This plateau is a time, often more than 100 days long, where the magnitude of the SN is almost constant, very slowly declining compared to right after the peak or right after the plateau, as seen in Figure 2.

The plateau is believed to arise because of hydrogen recombination: the hydrogen in the shell that was previously completely ionised by the shock wave, is expanding and cooling. This allows the hydrogen to re-capture electrons and become neutral hydrogen in a wave propagating inwards through the expanding envelope called the receding front or 'recombination front'. This recombination front is where the temperature equals the recombination temperature of hydrogen. This recombination front marks the photosphere of the SNII because the cooler hydrogen outside the recombination front is optically thin, whereas inside the front the hydrogen is still ionised and therefore optically thick.

While this recombination front continues to recede, the ejecta simultaneously continues to expand, and the temperature remains roughly constant at the recombination temperature. Meanwhile the radius also remains roughly constant. Now because both the radius and the temperature remain roughly constant, so does the photosphere and thereby also the luminosity leading to the plateau in the light curve. This plateau then lasts until the shock wave reaches the recombination front, marking

the point where the ejecta is fully recombined and thereby optically thin: the light from inside the shell can now escape.
This means that the duration of the optically thick period is the time from the initial explosion when the first hydrogen is ionised, until the end of the plateau when all of the hydrogen has recombined. The duration of the plateau is then the time from when the hydrogen becomes cold enough to start recombining, until all of the hydrogen has recombined.
This leads to the belief that the duration of the plateau is related to the mass of hydrogen in the envelope when the progenitor explodes. Therefore, a thicker shell should result in a longer plateau and vice versa. However, this tells nothing about whether the density of the shell might affect the duration of the plateau, only that the mass of the shell will affect it.

Furthermore, due to the enormous size of the RSG progenitors, they have very low surface gravity, causing extreme mass loss. The more massive ones lose mass more rapidly and the less massive ones lose it more slowly and due to the onion-like structure of the RSG, the mass lost is Hydrogen. Despite initial masses between 10-40 $M_\odot$ the differing mass loss rates result in progenitors with similar final masses at around $10M_\odot$ but instead different mass in their surrounding shells.[10]
Because of these different mass losses, we would expect to observe a broader distribution of plateau durations from hydrogen rich progenitors having expelled different amounts of material, and from progenitors with various amounts of mass loss and mass loss periods.
However, we do also currently observe many SNe with long plateaus up to hundreds of days, but only very few with plateau durations of 10s of days.[8]

1.4 The P-Cygni Profile

As previously mentioned, most of these SNe manage to retain a hydrogen envelope that is still present when they explode. When we obtain spectra for these SNe, the H_α lines usually appear with a P-Cygni profile.
These so-called P-Cygni lines appear around the observed central wavelength of H_α with a blueshifted valley and a redshifted mountain top, as seen on the left in Figure 3.

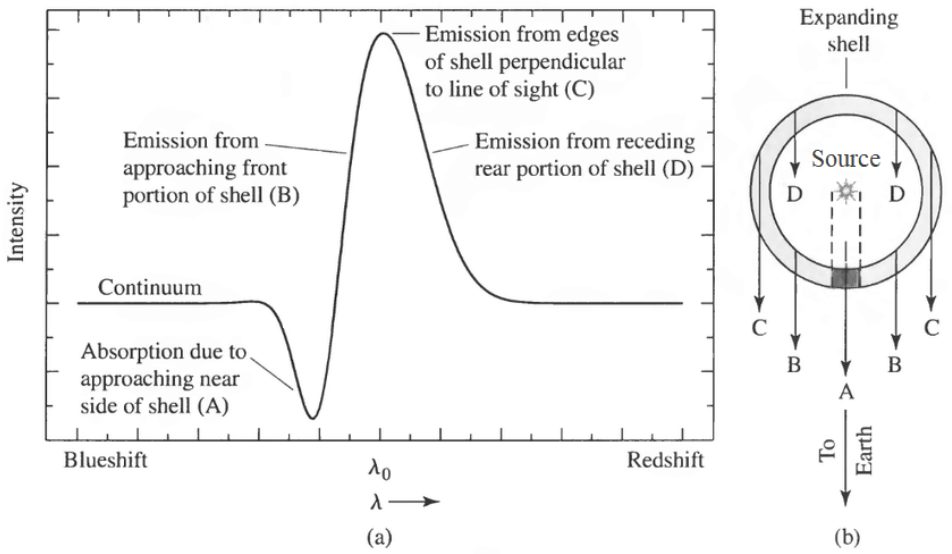

Figure 3: Illustration of the constituent parts of the P-Cygni profile.[11]

These lines are generated by a shell of gas moving outwards and away from the central light source, as seen on the right in Figure 3. The absorption, marked (A) in Figure 3, is blueshifted with respect to the rest-frame wavelength, because this comes from the optically tick material absorbing along the line of sight.
Meanwhile the emission lines come from three different parts of the shell. A part slighty blueshifted from the front part of the shell, marked (B), also approaching the observer. A part centered on the rest-frame wavelength, marked (C), comes from the edges of the shell that is perpendicular to the line of sight, and as this moves with the star it is not red- or blueshifted relative to the observer. The last part comes from the part that respective to the observer is behind the star, marked (D), and is therefore moving away from the observer.[11]

1.5 2020hgw: At First Glance

2020hgw was discovered on April 17th 2020 at a g-band magnitude of 17.95. Prior to this the last non-detection was April 5th 2020 at a g-band limit magnitude of 19.82. On April 28th 2020, it was classified with observations from the Nordic Optical Telescope(NOT). It was found to be a Type II SN due to the presence of Hydrogen in the spectrum, but since the classification occurred before the light curve had

declined sufficiently to reveal whether it was a type IIP or IIL, the classification was limited to type II.
It was found in the YSE Field 719.A at RA: 14:18:19.20, DEC: +38:55:46.42 within host galaxy SDSSJ141819.08+385546.1. The redshift is 0.043241 with a luminosity distance of 190,202 Mpc and the SDSS photometric redshift is 0.041.

Several spectroscopic follow-up observations were made after the initial discovery, all observations 30 days prior to and 140 days post peak are included in Figure 4. At around 100 days we see a dramatic drop in the flux which then falls below the detection limits of the surveys, resulting in no useful observations after this. However, the data suggests a steady decline prior to this, and having later data than this should not make a difference to the appearance of the radioactive tail, nor the light curve.

1.6 Why is 2020hgw Interesting?

What is remarkable about 2020hgw at first glance are two things. First of all, it is very bright: other SNe peaking above an absolute magnitude of -18 are marked as luminous[8], and 2020hgw peaks at almost -19.
Additionally in some bands, the light curve seems to exhibit a short plateau of less than 50 days. This is less than some of the shortest plateaus measured to this day[8], and we see it in multiple bands for 2020hgw.

Therefore in this thesis I will go on to investigate the properties of this SN and compare it to the existing population of type II SNe. I will do this by fitting the light curve to be able to measure the length of the plateau, the duration of the optically thick phase, the time at which the SN transitions from decline to the plateau, the time at which the plateau ends, the time at which the SN has transitioned into the radioactive tail, the slope of the decline from the peak, and the slope of the plateau. I will determine the magnitude at the peak, at 30 days prior to the middle of the radioactive tail and at 30 days after the middle of the radioactive tail.
I will measure the total radiated energy.
Last, but not least, I will measure the emission and absorption velocities of the H_α P-Cygni profile lines and the absorption over emission coefficients for spectra at four different epochs.

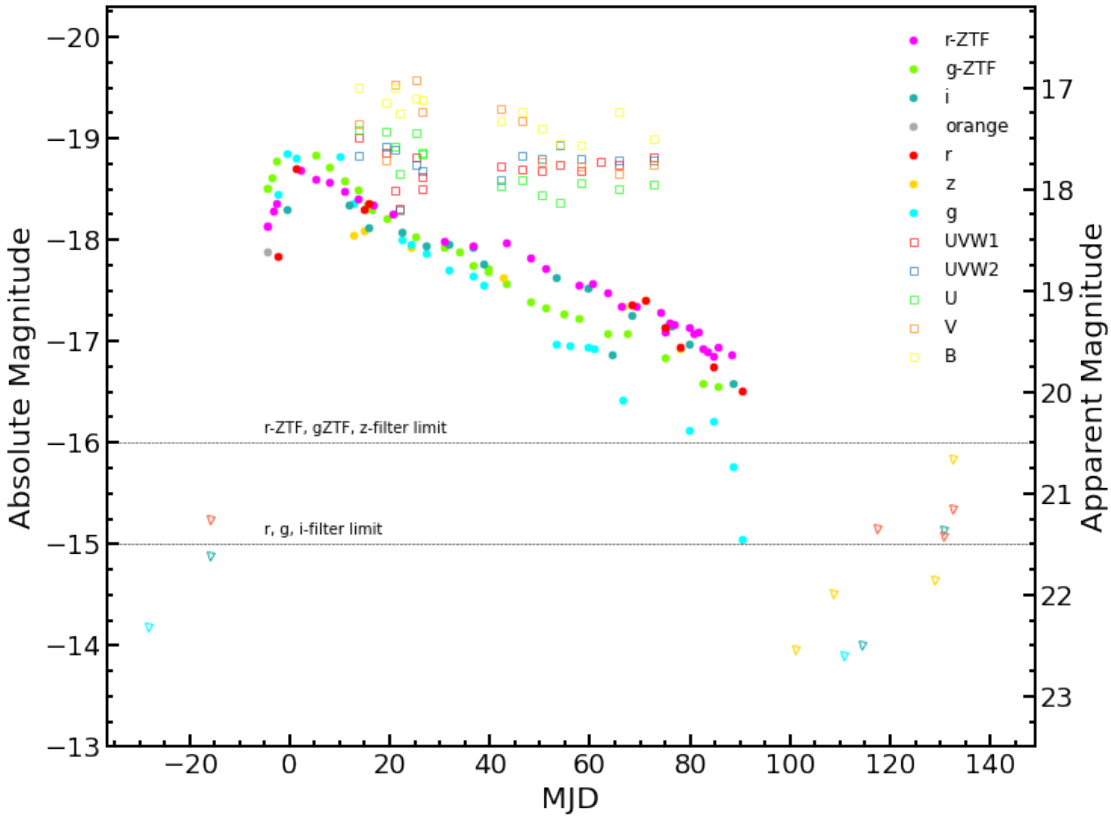

Figure 4: Light curve of 2020hgw 30 days prior to M_{peak} until 140 days post M_{peak}. Unfilled triangles depict data points that are outside the limit magnitudes for the different filters. Squares depict data points that had not, and could not be host-galaxy corrected. The time origin is set to the peak magnitude in the r-ZTF band.

2 The Data

2.1 2020hgw: Photometric Data

2.1.1 ZTF

I use Zwicky Transient Facility(ZTF) public survey data, these are marked with r-ZTF and g-ZTF in Figure 4. The ZTF survey uses the Palomar 48 inch (1.2 m) Samuel Oschin Schmidt telescope with a 47 square degrees field of view, observing up to 3760 square degrees per hour. It employs custom g-, r-, and i-filters with a detection limit in r of 20.5 mag for a 30 second exposure. The ZTF public survey covers the entire visible sky from Palomar every three nights.[12]

2.1.2 YSE

2020hgw was found in a YSE field and is part of the Young SN Experiment(YSE). YSE is a three year survey focused on discovering young transients, and on building statistical samples of transients. YSE began on November 24th 2019, using 7% of the Pan-STARRS1 observing time, surveying 750 square degrees of sky every 3 days. The Pan-STARRS observations are taken through four different broadband filters: g, r, i, z with 27 second exposure times each. It is able to do this at a depth of 21.5 mag in the g, r and i filters, and 20.5 mag in the z filter in a single observation.[13] Together the four filters cover the wavelengths from approximately 4000-9300 Å.[14] The observing strategy of YSE also takes the moon into account by rotating the filters. When the moon is full, i.e. very bright, they alternate between r&i and r&z. When the moon is less full, i.e. grey, they alternate between g&i and g&z and when the moon is new, i.e. dark, they alternate between g&r and g&i.[13] However, this sometimes results in gaps of over a week for certain filters, as can be seen for for example the r-band in Figure 4.

The telescopes used are the two Pan-STARRS telescopes: Pan-STARRS1 and Pan-STARRS2. Both are 1.8 meter telescopes with 1.4 gigapixel cameras and an approximately 7 square degrees field of view. The calibration of PS1 has been upgraded multiple times to a precision better than 5 mmag, which essential to SN cosmology.[13]

Combining Pan-STARRS observations with alternating observations from ZTF, YSE

obtains observations every one or two days when possible and the survey strategy emphasises increased coverage and depth in i and z.

2.1.3 ATLAS

I also used data from the Asteroid Terrestrial-impact Last Alert System(ATLAS), that is tuned for observing asteroids close to Earth, but it has nonetheless observed many other objects. ATLAS observes a significant portion of the sky every other night covering 1/2 of the visible sky per night, and with a two day cadence, the full visible night sky. ATLAS is able to confidently observe this down to about 19.5 mag[12] with 30 second exposures, making available additional high cadence observations of 2020hgw among many other SNe.[15]
The ATLAS c-filter covers the wavelengths from 4200-6500 Å and the o-filter covers 5600-8200 Å, effectively covering the same wavelengths as the four PS1 filters mentioned above.
In Figure 5 data for the ATLAS o and c filters is shown. For these filters there were also several data points that were already marked as being outside the magnitude limits and therefore not data to be used in the analysis. These points are shown as unfilled triangles with the blue points presenting the o-filter and the red presenting the c-filter.

2.1.4 SWIFT

A Swift follow-up programme was triggered for 2020hgw to obtain UV and U,V,B band photometry after maximum light. For this Swift uses the Ultraviolet/Optical Telescope(UVOT) which operates in the 1600-8000 Å range. This has broad-band filters in both the ultraviolet(UVW1, UVW2, UVM2) and optical(UVB) to obtain colour information.[16]
These observations can be seen in Figure 4 as the unfilled squares between days 10 and 80.
However, without pre- or post-supernova photometry, it is not possible to perform corrections of the host galaxy contribution to the brightness of these points.

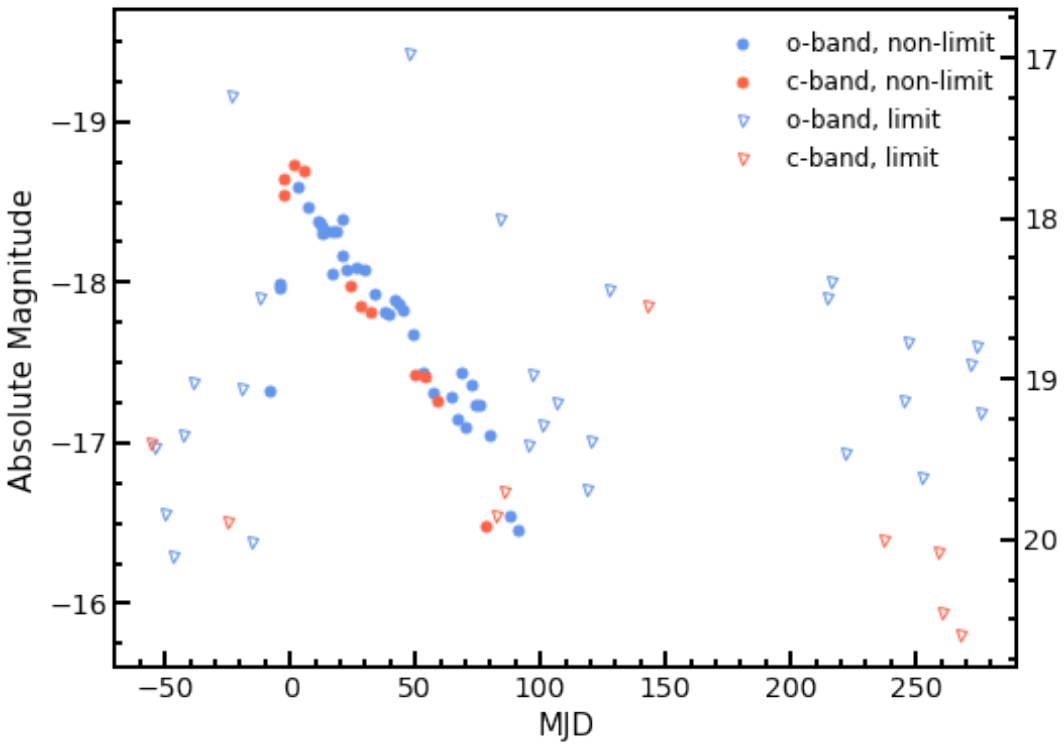

Figure 5: ATLAS o and c filter data, marked according to limit or not limit.

2.2 Photometric Data Utilised

In Figure 4 all data for 2020hgw is shown from 30 days prior to 150 days post peak, but many data points are marked with unfilled triangles. At the top are shown the U, V, B, UVW1 and UVW2 filters which come from SWIFT photometry but this data has not been host galaxy corrected. Since we have no way of estimating the host galaxy luminosity in these bands however, these data points are discarded in the analysis.

At the bottom of Figure 4 are data points marked with unfilled triangles. These points are at the upper limits of the different filters and come from non-detections of the object. This means that if there at these points is any light to be detected from the supernova, we can not confidently detect it at these magnitudes. The points belong to the Pan-STARRS g, r, i and z filters and the limits are marked by horisontal, dashed lines.
Furthermore, the r-filter data which is what could have been used for fitting the plateau has no observations during the plateau that we see in other filters, due to the lunar dependent observing strategy, making it less of a loss than it could have been. The same is true for the z-filter data as this is also very poorly sampled.

I choose not to use the PS1 r and g band observations altogether, because filters from different telescopes and surveys have different transmissions, which leads to subtle differences in the photometry. Differences that in the end could affect the fits made to the light curve. I therefore choose to use the ZTF data for the r and g filters as they are more well sampled due to the lunar dependent observing strategy of PS1.

The data has now been cut to five different filters: r-ZTF, g-ZTF, i, c and o as can be seen in the light curve in Figure 6. Shown are the absolute magnitudes and the observed apparent magnitudes, from first non-detection to 89 days after peak magnitude with the Modified Julian Date normalised to have origin at the peak. These are the data points that were used for computing the bolometric light curve and for fitting to the light curve.

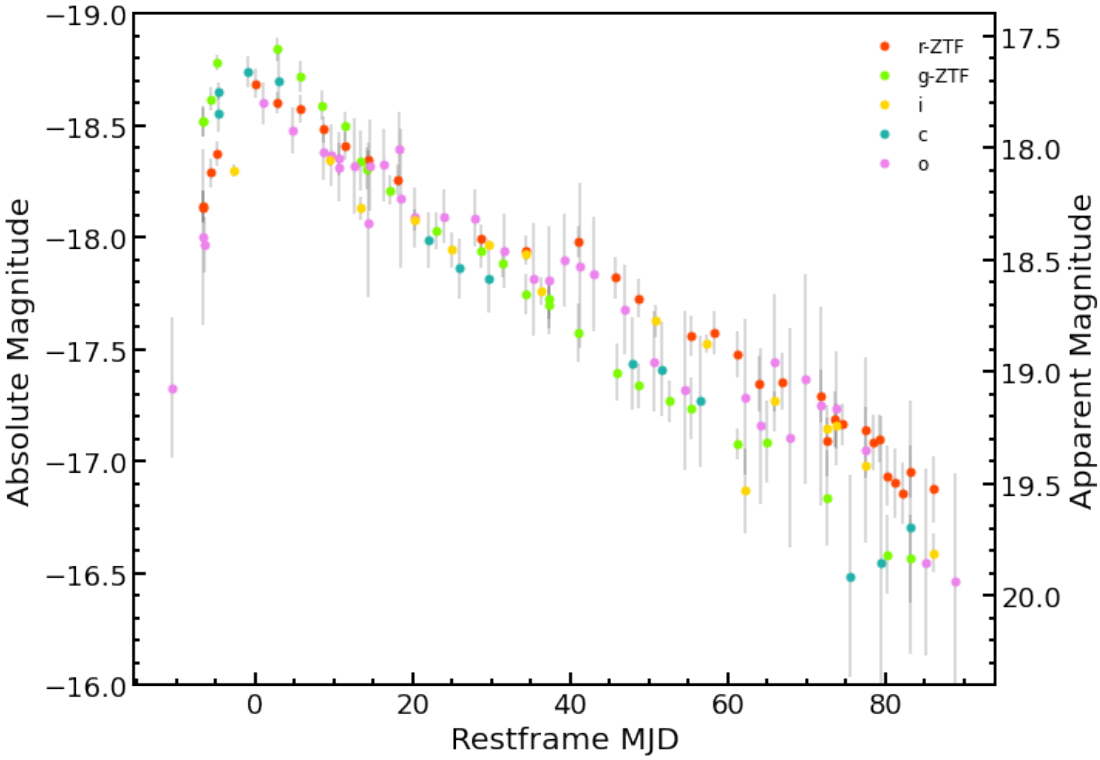

Figure 6: Light curve of 2020hgw 10.5 days prior to M_{peak} until 89 days after. The time origin is normalised to the peak magnitude in the r-ZTF band.

2.3 2020hgw: Spectroscopic Data

Four of the five obtained spectra were observed with the Nordic Optical Telescope(NOT), using the Alhambra Faint Object Spectrograph and Camera(ALFOSC). The normalised spectra are shown in Figure 7 in chronological succession with the earliest spectrum at the top in orange and the last spectrum at the bottom in purple. The convolved spectra are plotted over the original spectra for clarity and to make it easier to see the features.

The first spectrum was observed on 28/04/2020. It was observed with grism 4, which covers the wavelengths range from 3200-9600 Å, and has a central wavelength of 5800 Å. Furthermore the 1" slit was used, giving a resolution of $R = 360$.

The second spectrum was observed on 23/05/2020 and was used to classify 2020hgw as a Type II. It was observed using the KAST spectrograph of the Shane 3-m Telescope. The telescope is optimised for both the blue and the red wavelengths, but for these observations grating 6 was used. This grating has 300 grooves, a blaze at 7500 Å, and a useful wavelength range of approximately 3800-11000 Å, the widest range of the spectra as seen in Figure 7. For this observation the 1" slit was used.[17]

The third, fourth and fifth spectra were observed on 28/05/2020, 09/06/2020 and 19/07/2020. All three were observed using ALFOSC and grism 8 which covers the wavelength range from 5680-8580 Å and has a central wavelength of 7030 Å. All were observed using the 0.5" slit with a resultant resolution of $R = 1000$. In Figure 8, there are six dashed lines. The furthest left one marks April 17th 2020 when 2020hgw was discovered. The following five, grey dashed lines mark the times when the above mentioned spectra were taken.

This shows that the 23/05/2020 spectrum is observed right at the start of the plateau, the 28/05/2020 spectrum is observed during the early parts of the plateau, and the 09/06/2020 spectrum is observed right around the end of the plateau.

It also shows that the 19/06/2020 spectrum is taken around the very last possible time before 2020hgw went behind the sun and became unobservable for a period.

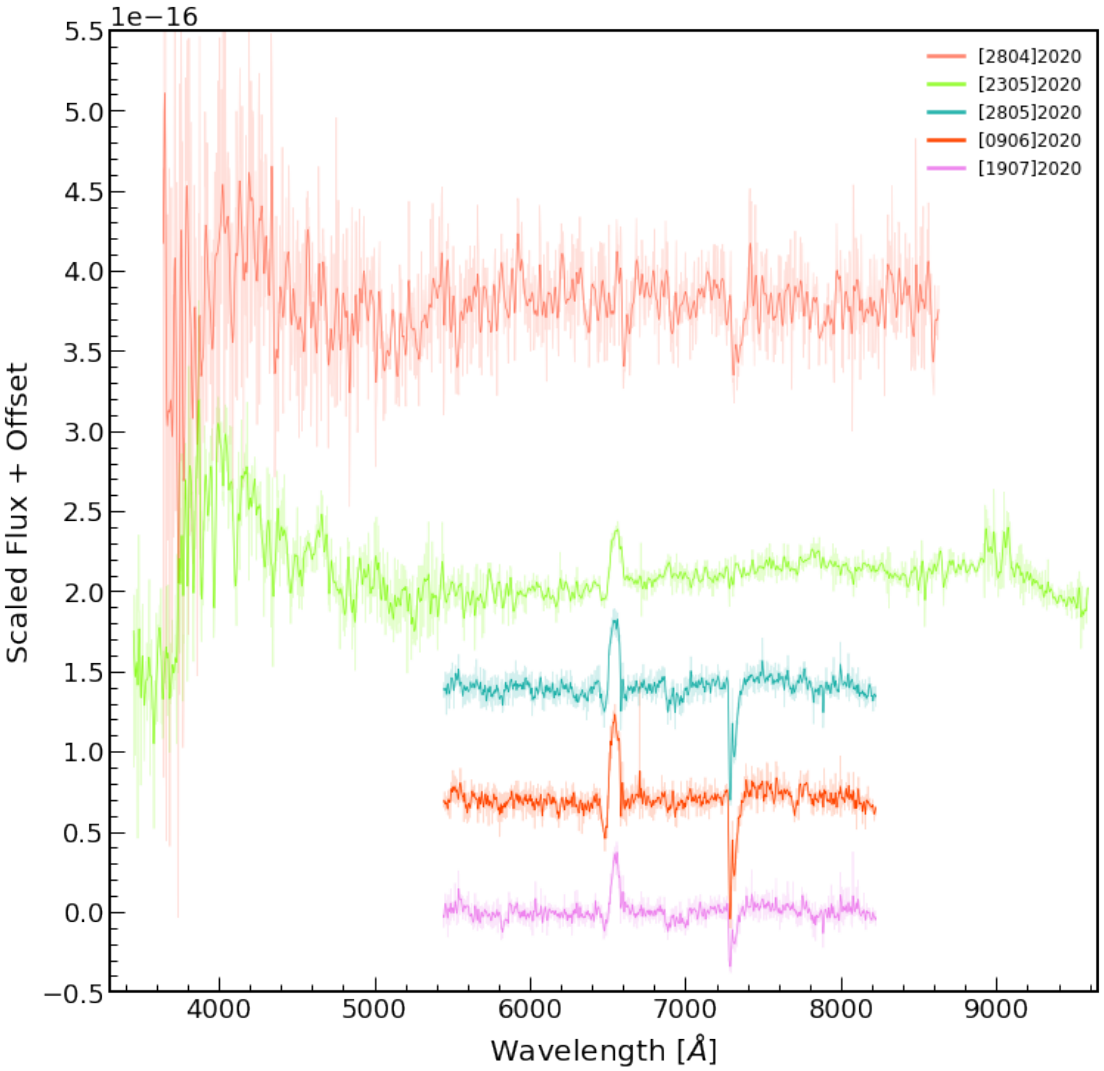

Figure 7: The five obtained spectra for 2020hgw in chronological order with the earliest spectrum at the top in orange, and the last spectrum at the bottom in purple. The convolved spectra are plotted over the original spectra for clarity and for the spectral features to be clearer. The top four spectra have each been offset upward to better illustrate the similarities in the bottom four spectra.

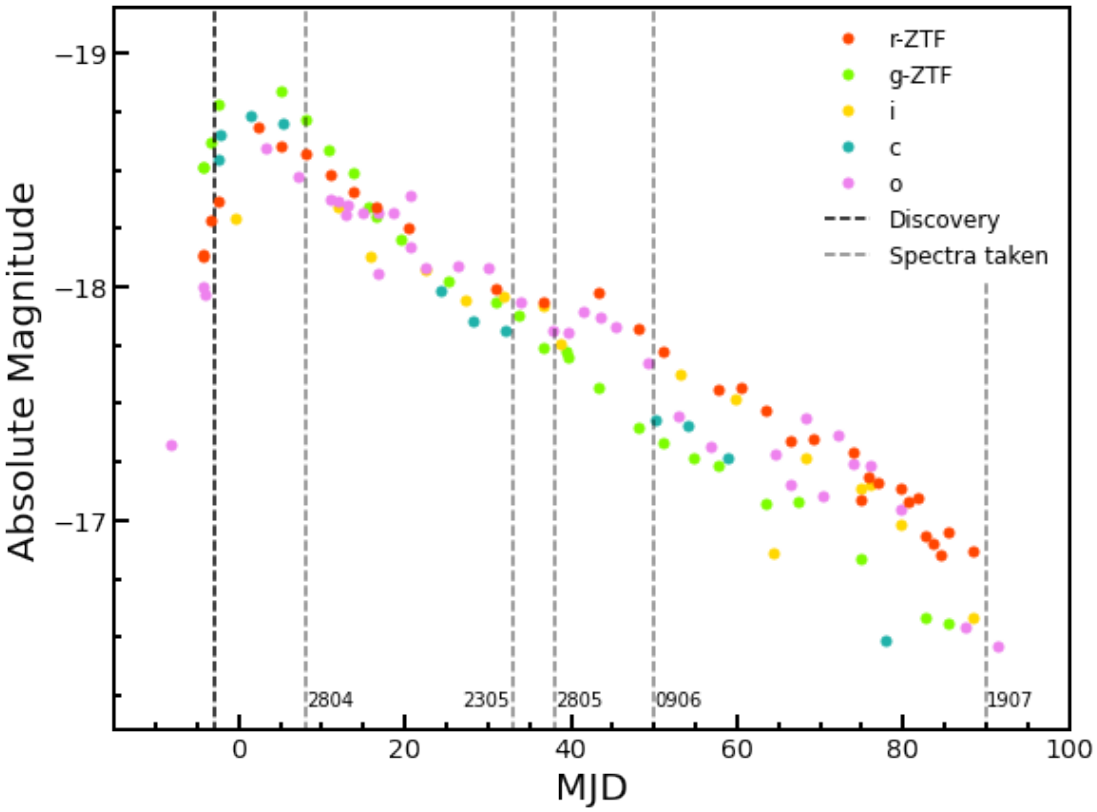

Figure 8: Dashed vertical lines indicating when on the light curve spectra were taken of 2020hgw.

2.4 The Comparison Samples

2.4.1 Anderson et al. 2014

To find out whether 2020hgw falls within a general population of Type IIP SNe, I compare it to two different samples. The first sample is the SNe analysed in Anderson et al. 2014[9]. They photometrically analyse a total of 116 Hydrogen-rich Type II SN for which they make several magnitude measurements, find the decline rates s_1 and s_2 and the time duration of the plateau and optically thick phase. They also apply Equation 19 to find t_{PT}.

Their SNe is a combination of V-band data of Type IIP and IIL SNe from five different SN follow-up programs: the Cerro Tololo SN program, the Calán/Tololo SN SN program, the Optical and Infrared Supernova Survey, the Carnegie Type II Supernova Program, and the Carnegie Supernova Project(CSP).[9] They do however exclude Type IIb and IIn SNe from their analysis, and purely look at Type IIP and IIL.

They choose to use V-band data as this has historically been the most used filter for observations of SNe, hence making it easier for them to compare to previous papers. Additionally their SNe show better coverage in the V-band filter.

2.4.2 Gutiérrez et al. 2014

In that paper Gutiérrez et al. 2014 make a spectroscopic analysis of V- and B-band data for 52 Hydrogen-rich Type II SNe. These 52 are a subsample of the Anderson et al. 2014 sample, and are only the ones they were able to perform spectral analyses on. They focus on the H_α P-Cygni profiles, specifically on the emission velocity from the FWHM and the absorption equivalent width over emission equivalent width(a/e) coefficient. They perform these measurements on spectra at the beginning of the recombination phase, i.e. at t_{tran} + 10 days.
They also measure s_1, s_2, M_{max} and OPTd following the same methods as Anderson et al. 2014.

3 Methods

In this section I dive into exploring the properties of 2020hgw to be able to compare it to the Type IIP population. I do this by measuring the following:
Total radiated energy, the time at the middle of the transition into the radioactive tail t_{PT} and the magnitude at peak, end of plateau and at the radioactive tail.
I also find the duration of the optically thick phase and the plateau along with the times at which the transition to the plateau happens and when the plateau ends.
Then I fit the slope of the first decline and the plateau and statistically and visually inspect these.
Last, but not least, I make fits to the H_α lines at the four different epochs to measure the velocities of the absorption and emission, and the relative equivalent widths of the absorption to emission.

For all of the photometric data I calculated the absolute magnitudes for 2020hgw according to Equation 1:

$$M = m - 5 \cdot (log_{10}(d) - 1) \tag{1}$$

Where M is the absolute magnitude, m is the apparent magnitude and d is the luminosity distance.

3.1 Superbol

`Superbol` is a python program used to calculate the bolometric luminosity of SNe. For this it uses a set of apparent or absolute magnitudes in up to several different filters.[18]
Prior to running `superbol` I calculated the extinction corrections to each filter

according to the following equations:

$$E(B-V) = 0.011 \tag{2}$$
$$ext_u = E(B-V) \cdot 4.786 \tag{3}$$
$$ext_g = E(B-V) \cdot 3.587 \tag{4}$$
$$ext_r = E(B-V) \cdot 2.471 \tag{5}$$
$$ext_i = E(B-V) \cdot 1.798 \tag{6}$$
$$ext_z = E(B-V) \cdot 1.403 \tag{7}$$
$$ext_U = E(B-V) \cdot 4.744 \tag{8}$$
$$ext_B = E(B-V) \cdot 4.016 \tag{9}$$
$$ext_V = E(B-V) \cdot 3.011 \tag{10}$$
$$ext_A = E(B-V) \cdot 6.432 \tag{11}$$
$$ext_S = E(B-V) \cdot 9.270 \tag{12}$$
$$ext_c = E(B-V) \cdot 3.111 \tag{13}$$
$$ext_o = E(B-V) \cdot 2.185 \tag{14}$$

I then ran `superbol` on the photometric data from the r-ZTF, g-ZTF, i, o and c bands after correcting for line of sight extinction.

The process of calculating the bolometric luminosity with `superbol` is an interactive process. First I had to choose which bands to use for the process and which filter I wanted to use as the reference filter for sampling epochs. Here I chose the r-band as it is best to use data from a filter with many observations in order to improve sampling over the light curve for the rest of the filters.
`Superbol` then prompts for the redshift of the SN, whether to correct for time dilation and whether the magnitude it has found for the reference filter is correct.
After this I went through fitting each filter with different order polynomials and whether to extend the fit using constant colour, a polynomial or a combination of both for extrapolating early and late times.
`Superbol` then fits to all the given filters and the interpolated light curves to produce a total bolometric light curve, while assuming that the object behaves like a black body.

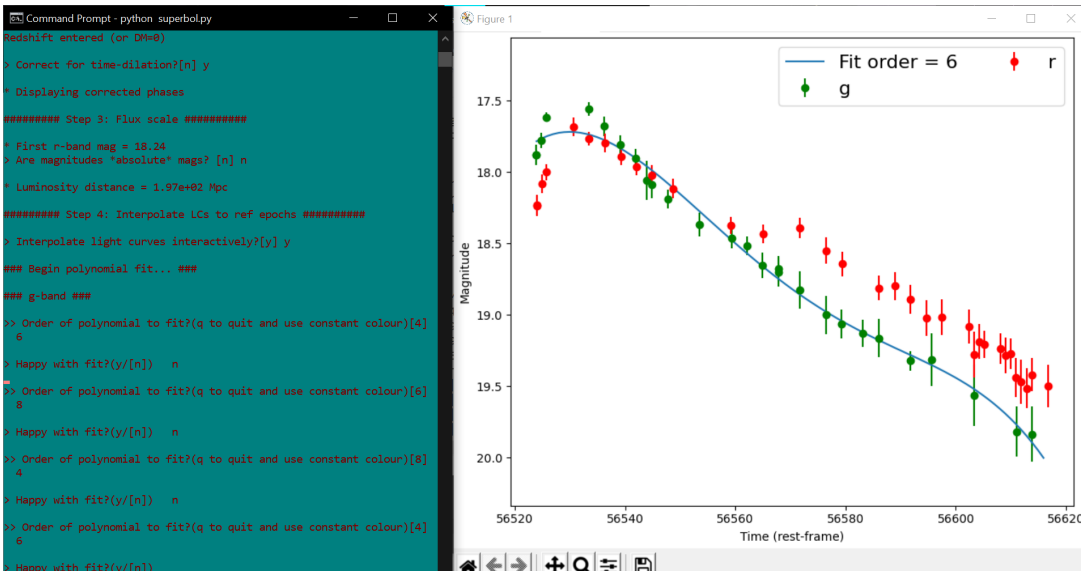

Figure 9: The process of finding the best possible polynomial fit for the g-filter with superbol. Behind the g-filter data is the r-filter data that was chosen as the reference filter each time.

In Figure 9 is shown an example where I am finding the right polynomial for the g-filter data and behind the g-filter data is the r-filter data that was used as the reference filter. From resulting bolometric light curve I am able to integrate under this curve to find the total radiated energy.

3.2 Olivares and the Curve

For a typical IIP SN, the light curve consists of a few distinct parts. First a short approximately 7-10 day rise time, the peak, then a period of decline which transitions into a plateau of almost constant magnitude typically lasting around 70 to more than 100 days, before finally transitioning from the plateau into the radioactive tail.

To describe the photometric behaviour of a Type IIP SN we can use a model which treats the individual components of the light curve separately. This is why, for examining the properties of the light curve of 2020hgw, I used Equation 4 in Olivares et al. 2010[19]. This function has no physical interpretations however, and is a purely analytical function used to model the light curve.

Though in the end, fitted to the light curve in unison and not by parts, it is comprised

of three parts that fit to separate parts of the light curve.
The first part(green dashed line in Figure 10) is a Fermi-Dirac function:

$$f_{FD}(t) = \frac{-a_0}{1 + e^{(t - t_{PT})/w_0}} \tag{15}$$

Here a_0 is the height of the step in units of magnitude, t_{PT} is the time at the middle of the transition phase and w_0 is the width of the transition phase in days. This provides a good description of the part of the light curve that transitions from the plateau to the radioactive phase.
The second part is a straight line(magenta dashed line in Figure 10):

$$l(t) = p_0 \, (t - t_{PT}) + m_0 \tag{16}$$

where p_0 is the slope of the radioactive tail in units of magnitude per day, and m_0 corresponds to the magnitude at t_{PT}. This part models the slope of the radioactive decay after the plateau.
The third part is a Gaussian function(blue dashed line in Figure 10):

$$g(t) = - P \, e^{-\left(\frac{t-Q}{R}\right)^2} \tag{17}$$

where P is the height of the peak of the Gaussian in units of magnitudes, Q is the center of the Gaussian in units of days, and R is the width of the Gaussian in units of days. This part of the function describes the light curve curvature during the plateau.
The resulting analytical function in Eq. 19 has eight free parameters and can be used to fit the light curve in unison. The resulting analytical function is given as:

$$F(t) = f_{FD}(t) + l(t) + g(t) \tag{18}$$

$$= \frac{-a_0}{1 + e^{(t - t_{PT})/w_0}} + p_0 \, (t - t_{PT}) + m_0 - P \, e^{-\left(\frac{t-Q}{R}\right)^2} \tag{19}$$

One thing to note however is, in the article from 2010, the SNe they sample mostly don't have any data until after the peak. This means that they use the Gaussian to model the curvature of the plateau, whereas we do have that data for 2020hgw and it therefore made more sense to model it with the Gaussian accounting for the

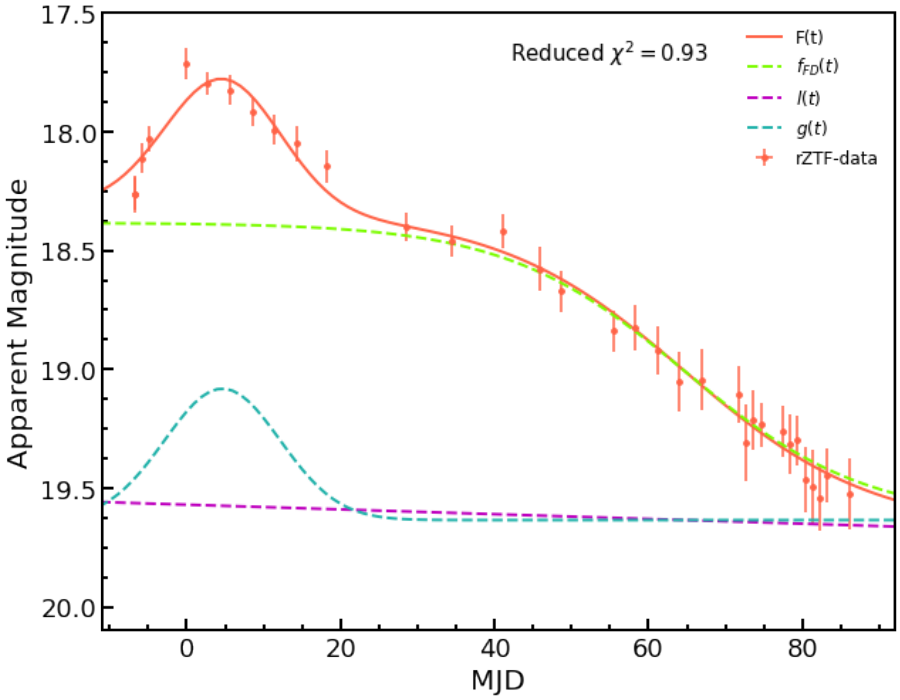

Figure 10: The three parts of the analytical equation used to fit the light curve: $F(t) = f_{FD}(t) + l(t) + g(t)$, shown separately and combined with $F(t)$ and rZTF-data in solid red, $f_{FD}(t)$ as dashed green, $l(t)$ as dashed magenta and $g(t)$ as dashed blue.

peak. In Figure 1 in Olivares 2010[19] they also show that they do the same for the B-band data, but not for V, R and I.

3.3 Anderson et al. 2014

Anderson et al. 2014 define some different parameters to describe the light curve, with some of them being based on the fitting according to Equation 19, which provides t_{PT}.

Figure 11 shows the different parameters Anderson et al. 2014 calculate for the SNe in their sample. M_{max} is the initial peak in the V-band light curve. For their data, often they do not have data early enough to be the actual peak, and they use the first photometric point, whereas we do have data prior to and around the peak.

We do however not have any V-band data and are unable to make the k-correction due to a lack of spectral coverage at the necessary epochs for 2020hgw. I therefore

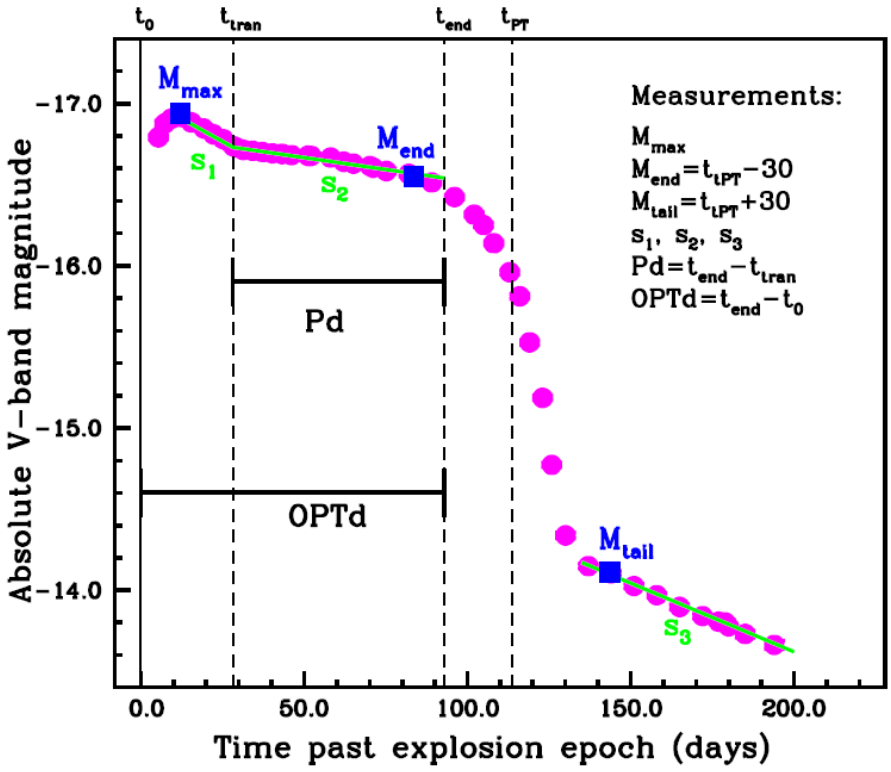

Figure 11: Figure 1 from Anderson et al. 2014[9]

instead find this and the following parameters for the r-ZTF-band.

M_{end} is defined as the absolute magnitude 30 days *before* t_{PT} which is supposed to represent the end of the plateau.
M_{tail} is defined as the absolute magnitude 30 days *after* t_{PT}. This is supposed to represent the magnitude right after it has transitioned into the radioactive decline.
s_1 is defined as the slope of the steeper decline in magnitude from the peak to the beginning of the plateau, in units of magnitudes per 100 days.
s_2 is defined as the slope of the less steep decline in magnitude of the plateau, also in magnitudes per 100 days.
$Pd = t_{end} - t_{tran}$, the plateau duration, where t_{end} and t_{tran} are the beginning and end of the plateau. More specifically t_{tran} marks the transition from s_1 to s_2 or the transition from decline to plateau. t_{end} marks the end of the plateau or the transition from plateau to the radioactive tail.
$OPTd = t_{end} - t_0$, the optically thick phase duration. Here t_0 is the explosion epoch: sometime between the last non-detection and the first detection of a rising magnitude.

3.4 The Fitting Process and Other Side Quests

3.4.1 Fitting the Light Curve

Using Equation 19 I went on to fit the light curve of 2020hgw. As it did not appear with a plateau in all of the filters, the fitting was performed on the r-ZTF data alone. This was done using the `Python` package `lmfit`. From `lmfit` I used `minimize` with the '`leastsqr`' method and a self-defined χ^2 function defined to include all of the parameters. I also used `Parameters` to be able to define a value and upper and lower bounds for each of the parameters used in the fitting. It also allowed me to print each of the values and their uncertainties(standard deviations from the median) after the fitting, to inspect whether they made sense or if I needed to change the bounds. Using the `minimize` function also allowed me to print a χ^2 value for the fit to inspect whether the fit made sense statistically and not just visually. Last, but not least, I would plot the fit on top of the data in between adjustments to see whether the model actually fitted a plateau and peak resembling the behaviour of the data.

3.4.2 Fitting s_1 and s_2

From the fit to the light curve I was then able to analytically find values for t_{tran} and t_{end} by finding the point of inflection of the curve. This is where the sign of the curvatures changes and in this case the transition from decline to plateau, and plateau to tail.

This was done by first interpolating according to the model using the parameter values from the fit, along the curve where the transition points would be. Then, finding the second derivatives of the points in two parts:

$$dot = \left(\frac{y'}{x'}\right) \tag{20}$$

$$dotdot = \left(\frac{dot'}{x'}\right) \tag{21}$$

Now with $dotdot$, I find the point $dotdot_i$ on the curve where the absolute difference between $dotdot_i$ and $dotdot_{i-1}$ is smaller than the difference between $dotdot_i$ and $dotdot_{i+1}$:

$$t_{tran} = x_i \; given \;\; |(dotdot_i - dotdot_{i-1})| < |(dotdot_i + dotdot_{i+1})| \tag{22}$$

The same procedure was then followed for finding t_{end}.

For fitting s_1 and s_2 I used `Minuit` from the `iminuit` library and an upgraded version of `probfit`'s χ^2 regression function. Using `Minuit`'s `migrad` I was able to perform a fit to the data with a linear function, and then see the fitted values, whether `Migrad` was able to find a minimum and perform the fit and how good of a fit it was.

I made four different fits for s_1 and s_2 according to the different methods of approach stated in Anderson et al. 2014[9]. I fit them as two separate lines and as a single line according to the paper. I also fit the plateau as a separate s_2 using values of t_{tran} and t_{end} found by visual inspection of the light curve to find the parts that look to be strictly part of the plateau.

As an aid in judging which value for s_2 to use in the further analysis, I calculated the Bayesion Information Criterion(BIC) score for each of the fit methods. I did this using the `RegscorePy` library's package `bic`. The `bic.bic` command takes three

arguments when scoring your model: the actual values, the predicted values and the number of parameters used in the model. This score penalises complexity so as to not overfit, and the bigger the absolute value of the BIC score, the better the fit. I used this tool to calculate the BIC score of five fits: s_1 and s_2 separately, s_2 with the strictly, visually plateau points, s_2 as one fit to all points from peak to t_{end} and for the s_1 and s_2 as separate fits but scored as if they were one fit.

3.4.3 Fitting the H_α lines

For fitting the H_α absorption and emission lines in the spectra I used various packages from the `astropy` and `specutils` libraries and the `scipy.interpolate` function `UnivariateSpline`.

For each spectrum I went through the following: first the wavelengths are corrected for redshift to the rest-frame wavelengths. The spectrum is then flattened using `UnivariateSpline` to make it easier to fit the features by fitting the continuum and subtracting to normalise the spectrum. Then the fitting to the absorption and emission was done separately, first defining the model for each with `astropy`'s `Gaussian1D` model which takes a guess at the amplitude, mean central wavelength and standard deviation as inputs. Then actually fitting with `specutils`' function `fit_lines`, this takes the spectrum, the previously defined model and a window to fit within as inputs.

Then, using the fits to the lines I create 'spectra' for `specutils.analysis.equivalent_width` to measure the equivalent widths of the emission and absorption to find the a/e coefficient.

The uncertainties on the a/e were found by propagating the errors calculated for the uncertainty on a and e, which were found according to Equation 23:

$$\sigma_{EW} \simeq 1.5 \frac{\sqrt{f \cdot p}}{SN} \tag{23}$$

Here f is the FWHM of the spectral line in Å, p is the size of a pixel in Å and SN is the signal-to-noise ratio[20]. Since SN is defined as the flux divided by the error on the flux, and no errors were provided for the NOT-spectra(2805-1907), I set their error to be 0.1, and I therefore use SN = 10 for those three spectra.

Last but not least, I calculate the absorption and emission velocities by converting

the mean wavelength I get from the `fit_lines` fit, into a Doppler velocity. I then run the fit several times and take the mean of the outputted mean to be the central wavelength, and the mean of the outputted standard deviation to be the uncertainty on the wavelength.
I convert the velocities through Equation 24, where v is the velocity of the line, λ_0 is the restframe wavelength of H_α, λ_{obs} is the observed wavelength and c is the speed of light.

$$v = \frac{\lambda_0 - \lambda_{obs}}{\lambda_0} \cdot c \tag{24}$$

I then scale the uncertainty from the fit, as this cannot be directly converted to velocity, i.e., if the uncertainty on the wavelength is 2%, then the uncertainty on the velocity is 2%.

4 Results

4.1 The Plateau

When looking at the data from the different filters, the plateau is not present in all filters, which is to be expected. In Figure 12 however, it can be seen that the plateau is clearly present in both the i- and r-ZTF-filter. As mentioned earlier, these filters observe in the red and infrared wavelengths which is where we find the H_α emission and absorption lines at this redshift. The plateau is therefore only expected to be seen in these filters because the plateau comes from the recombining hydrogen in the envelope surrounding the SN when it explodes.

The plateau is most prominent in the r-band, and though appearing somewhat shorter, also clearly visible in the i-band. This could come down to a bad data point for either of the filters resulting in a shorter plateau than in the r-band or a longer plateau than what is seen in the i-band. Either way, it is undeniable that the data show a plateau, and with better sampling in these bands it would make it much easier to confirm the presence of the plateau.

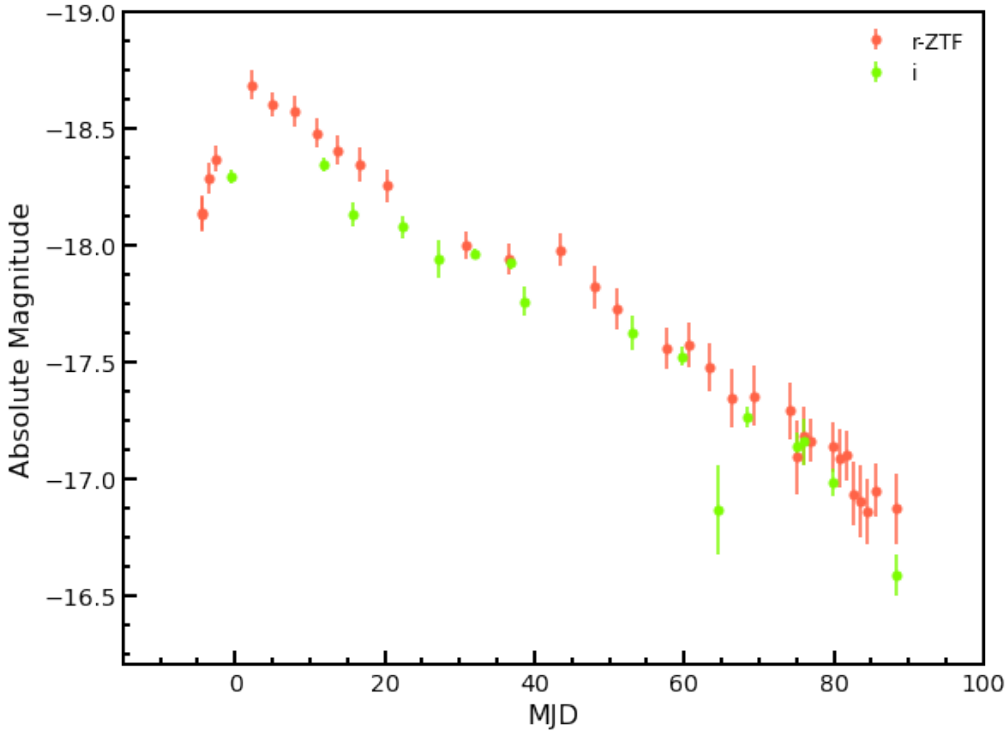

Figure 12: r-ZTF- and i-filter data both exhibiting a short plateau.

4.2 Fits to the Light Curve

Anderson et al. 2014 note that fitting this purely analytical model consistently provides good estimations of the time at which the transition between the plateau and the radioactive phase occurs, t_{PT}, though it does not always produce realistic values for the other parameters such as a_0 and p_0.
When fitting the light curve of 2020hgw I found a similar issue to Anderson et al. 2014. Some of the parameters were consistently fit to the limit values of the chosen, physically realistic, bounds, varying significantly. However, the value of t_{PT} remained consistently at $t_{PT} = 63.0 \pm 5$ and with a consistent uncertainty no larger than 6. This same problem is also noted by Anderson et al. 2014.

Though many of these fits produce reduced χ^2 values between 0.4 and 1 and therefore should be regarded statistically sound, visually and compared to the Anderson et al. 2014 sample, they produce unrealistic values for a_0, m_0 and p_0 in particular. Additionally, the uncertainties on these parameters become large and unconstraining.
In the end I obtained the fit shown in Figure 13.

The parameter values from that fit are:

$$
\begin{aligned}
a_0 &= 1.25 \pm 0.364, && bounds : [1.1,\ 2.5] \\
t_{PT} &= 64.76 \pm 5.66, && bounds : [30,\ 100] \\
w_0 &= 11.73 \pm 4.84, && bounds : [1,\ 150] \\
p_0 &= 0.001 \pm 1.21, && bounds : [0.001,\ 0.1] \\
m_0 &= 19.635 \pm 0.288, && bounds : [18.5,\ 20.5] \\
P &= 0.5533 \pm 0.0971, && bounds : [0.2,\ 5] \\
Q &= 4.652 \pm 0.617, && bounds : [-10,\ 30] \\
R &= 10.63 \pm 1.76, && bounds : [3,\ 50]
\end{aligned}
$$

For this fit the reduced $\chi^2 = 0.93$ making it compared to the other attempts, the statistically best fit, but also the visually best fit. As seen in Figure 10, marked by the dashed, blue line, the Gaussian part of the fit fits to the peak and not the plateau.

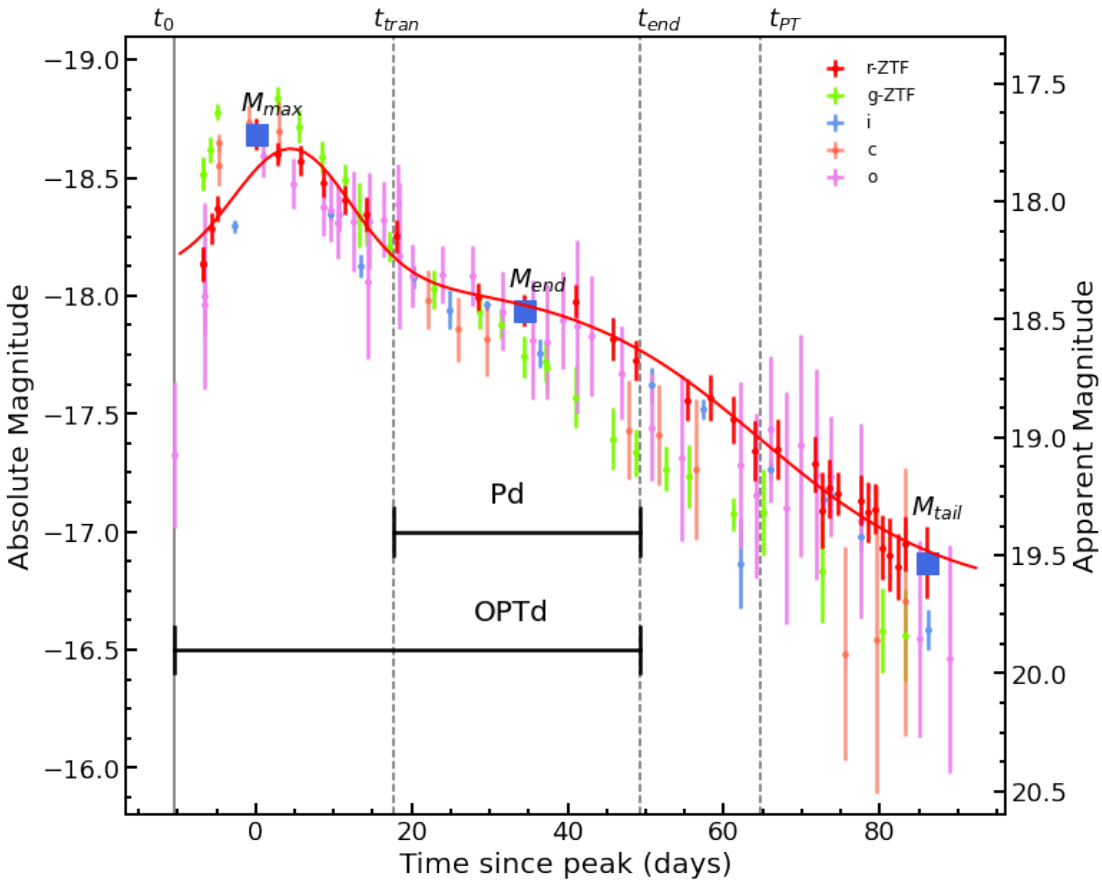

Figure 13: Replica of Figure 1 from Anderson et al. 2014[9], in red the fit to r-band data obtained using Equation 19 is shown. Data from five filters are shown in red, green, blue, orangered and purple. The vertical, lines show, in solid black the explosion epoch t_0, and in dashed black t_{tran}, t_{end} and t_{PT}. The horisontal black lines show Pd and $OPTd$. M_{max}, M_{end} and M_{tail} are shown with blue squares.

As I employ this fitting procedure purely for the measurement of t_{PT}, I go forward with a value of $t_{PT} = 64.76 \pm 5.66$.

4.3 Finding t_{tran} and t_{end}

Having obtained the fit described in the previous section, I go on to analytically try to determine t_{tran} and t_{end} as the points of inflection on the fitted curve. I therefore interpolated a set of y-values from the model and the obtained parameter values, and made a simple set of x-values to match. The boundaries I set for the two x-arrays were t_{tran}: [15, 35] and t_{end}: [25, 70].
I then used these arrays to find the second derivative of the curves in order to find the point at which the sign of the curvature starts changing. The values I find are:

$$t_{tran} = 17.60 \pm 0.47$$
$$t_{end} = 49.30 \pm 0.44$$

About these uncertainties - because the reduced χ^2 for the model as a whole was good despite the uncertainty for specifically p_0 being 1210 times larger than the value itself, when propagating for an uncertainty on the values I set $\sigma(p_0) = 0$. I do this because as previously stated, the only reliable value to extract from the fit is t_{PT} whose uncertainty is reasonable. Furthermore, p_0 comes from the linear part describing the radioactive tail, and is comparatively unimportant in the curves describing the transitions.

Do I not set the uncertainty for p_0 to 0, the values become $t_{tran} = 17.60 \pm 57.07$ and $t_{end} = 49.30 \pm 18.71$ which are enormous uncertainties, especially for t_{tran}, and when looking at the contributions from each of the parameter uncertainties, the uncertainty on p_0 accounts for 99% of it.
Additionally Anderson et al. 2014[9], to whom I compare the properties, do not describe how they measure these points and likely do this by eye. Therefore it is of lesser importance that this is not well constrained.

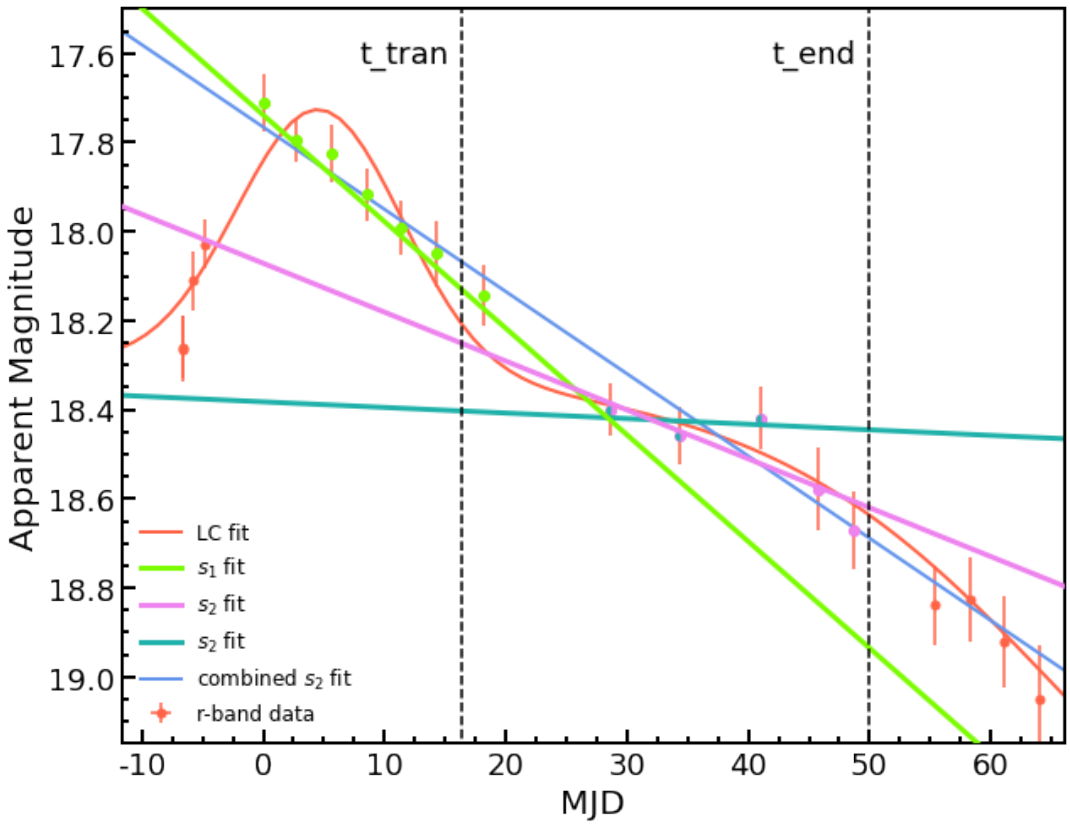

Figure 14: Linear fits to s_1 and s_2 separately in green and purple respectively, and a combined fit of s_2 in blue. In red are the r-band data and the light curve fit to the r-band data. In vertical, dashed, black lines are presented the calculated values of t_{tran} and t_{end}

4.4 The Fitting of s_1 and s_2

In order to compare 2020hgw to the Anderson et al. 2014[9] sample, I needed to make linear fits to s_1 and s_2. In the paper they state two different ways to fit the slope of s_2. Either as a combined linear fit to all data points from M_{peak} to t_{end}, or as two linear fits; s_1 and s_2 representing the slope of the decline from peak to plateau, and the slope of the plateau respectively. I chose to fit both ways to compare the methods.

For the separate s_2 fit I also made two versions. One fit using the analytical t_{end} as the end boundary, and one where I visually inspected which points really seem to make the plateau.

In Figure 14 s_1 is presented in green, the two s_2 fits are presented in purple and turquoise, and the combined fit is presented in blue.

Two ways to determine which is the better method can be applied however. Visual inspection of the fit against the data and BIC scores that analytically test the predicted values against the actual data. Visually, splitting it into two separate fits seemed to make the better fit, however, as they do in Anderson et al. 2014[9], I did still calculate the BIC scores for the two main scenarios:

$$BIC_{separate} = -66.08 \tag{25}$$

$$BIC_{combined} = -64.98 \tag{26}$$

Where $BIC_{separate}$ scores the s_1 predictions and s_2 predictions together, thouh the fits were made separately, and using t_{tran} as the end value. These fits are depicted with green and purple in Figure 14.
$BIC_{combined}$ scores the fit where all data points within the peak and t_{end} are fit as a single line, depicted by the thinner, blue line in Figure 14.
Now the more negative the BIC score is, the better, which tells us what we already knew: though not by a lot, the separate fits are better than a combined fit.

I did also score the two s_2 predictions against each other, just to make sure it was the right decision to use all five data points, and not only was it visually worse to only use the three data points, but the BIC score for using all five points was -25.8 and for the three points it was -20.5. Hence, there was no doubt that following the analytical boundary here was the right choice.

As can be seen in Figure 14 there is one more point of contention with this fitting. The seventh data point used in the s_1 fit is on the other side of the t_{tran} boundary. This is one of the times where a visual inspection of the data is important though because looking at the data, it is clear that the point is not part of the plateau. Instead including the point in s_2 would make the two slopes almost identical, despite them visually not being so. Furthermore, in Anderson (2014) it is stated that they also had to visually inspect the data in the process, sometimes even going against the BIC scores.

Following this, the obtained values for s_1 and s_2 are:

$$s_1 = 0.024 \pm 0.006$$
$$s_2 = 0.011 \pm 0.005$$

where the uncertainties are the given uncertainties from `Minuits migrad` that provides the Hesse error.

4.5 Anderson et. al 2014 and Their SNe

For comparisons with the Anderson et al. 2014 sample, and to replicate Figure 1 in the paper, I found the following values for 2020hgw:

$$M_{max(r-ZTF)} = -18.69 \pm 0.065$$
$$M_{end(r-ZTF)} = -17.93 \pm 0.066$$
$$M_{tail(r-ZTF)} = -16.87 \pm 0.151$$
$$Pd = 31.70 \pm 0.64$$
$$OPTd = 59.79 \pm 0.44$$

where the uncertainties on the magnitudes are the photometric errors given with the data, and the uncertainties on Pd and OPTd are propagated from the uncertainties on t_{tran} and t_{end}, and the uncertainty on t_0 is set to be 0 as this t_0 is taken as the day of the last non-detection and therefore does not come with an error.

Figure 13 is a replication of Figure 1 from Anderson et al. 2014[9] with the 2020hgw data. It shows in red the obtained fit to the r-ZTF-band data according to Equation 19. It also shows data from the five filters that had usable data. The dashed, vertical lines mark t_0, t_{tran}, t_{end} and t_{PT}. The two horisontal lines show the optically thick phase duration, OPTd, and the plateau duration, Pd. Furthermore, three magnitudes are marked: the maximum r-ZTF-band magnitude, M_{max}, M_{end} which is the magnitude 30 days prior to t_{PT}, and M_{tail} which is the magnitude 30 days after t_{PT}, with the latter representing the point where the SN has transitioned into the radioactive decline.

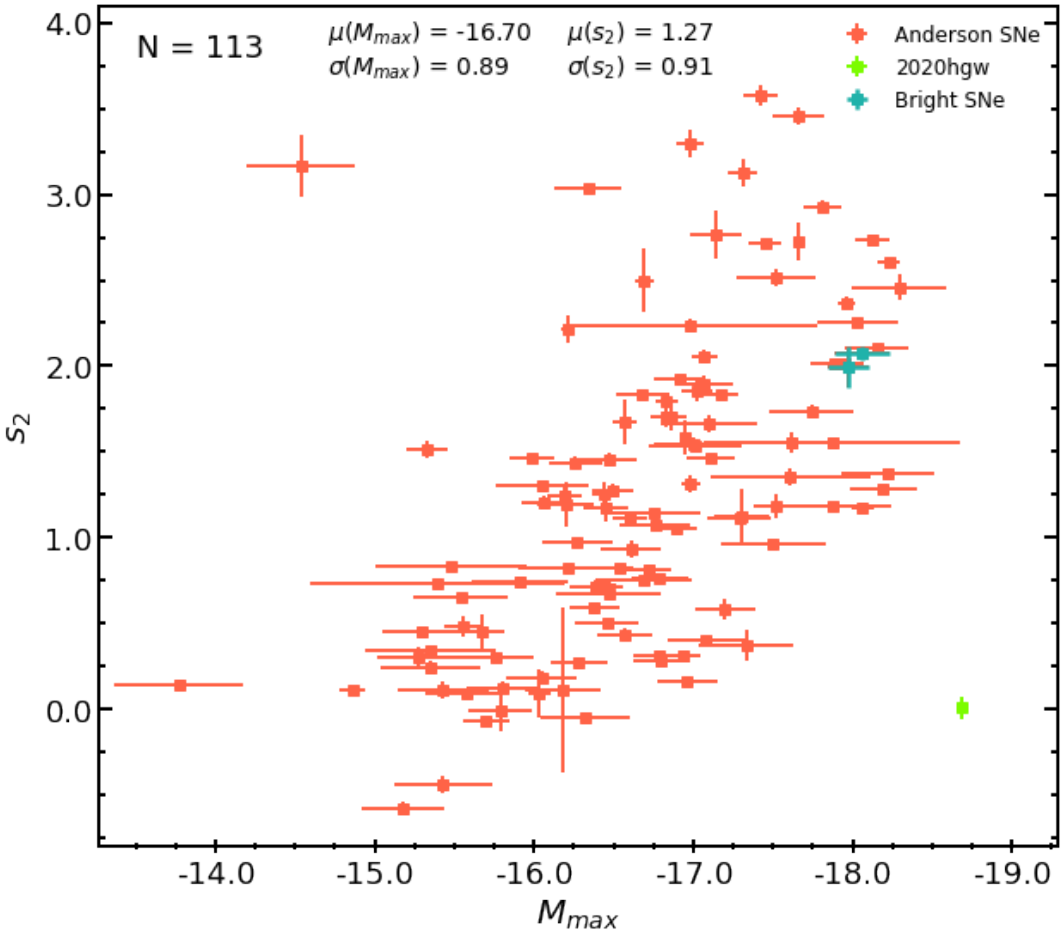

Figure 15: Maximum brightness, M_{max} versus slope of the plateau, s_2, for SNe from Anderson et al. 2014[9], and 2020hgw. SNe from Anderson et al. 2014[9] are marked in red, two remarkably bright SNe from that paper are marked in blue[8], and 2020hgw is marked in green.

In Figure 15, the maximum magnitude versus the slope of the plateau, s_2, is shown for 2020hgw and the 113 SNe in Anderson et al. 2014[9] that had data for both s_2 and M_{max}. Highlighted in blue are two SNe that have been marked as remarkably bright[8], like 2020hgw. A few outliers are seen on the opposite end from 2020hgw, but 2020hgw seems to lie alone in the lower right corner. However, the mean of s_2 for the Anderson et al. 2014 sample is 1.27, and the standard deviation is 0.91, which means that 2020hgw with an $s_{2(2020hgw)} = 0.011$, is only 1.38 σ away from the mean, which is not unreasonable.

It is here important to note, when making the comparison between the values obtained for 2020hgw and the values from Anderson et al. 2014 that they and later Gutiérrez et al. 2014 : they fit these values for the V-band data, whereas I am fitting to r-band data. I also don't apply a k-correction as there are too few spectra(covering a rather narrow wavelength range) to have the proper knowledge to do this, and this might affect the resulting comparisons. However, the ZTF r-band does overlap a significant portion of the V-band so regions of the spectral energy distribution should still be similar.

In Figure 16 the plateau duration, Pd, is plotted against maximum brightness, M_{max}, for 20 Anderson et al. 2014[9] SNe and 2020hgw. The SNe 2006Y and 2006ai are remarkably bright SNe[8] and are shown in blue. 2020hgw lies fairly close to 2006Y and 2006ai in plateau duration just as with brightness, and is only 1.19 σ away from the mean.

In Figure 17 the optically thick phase duration, OPTd, is plotted against maximum brightness, M_{max} for 71 Anderson et al. 2014[9] SNe. Here 2020hgw is also fairly close to the other two bright SNe in optically thick phase duration, lying 2.04 σ away from the mean.

4.6 Spectra and Spectral Fits

In Figure 7 the five observed spectra are shown chronologically, with the top spectrum in orange presenting the earliest observed spectrum that was used to classify 2020hgw, and the lowest spectrum in purple presenting the last spectrum observed, shortly before 2020hgw went behind the Sun.

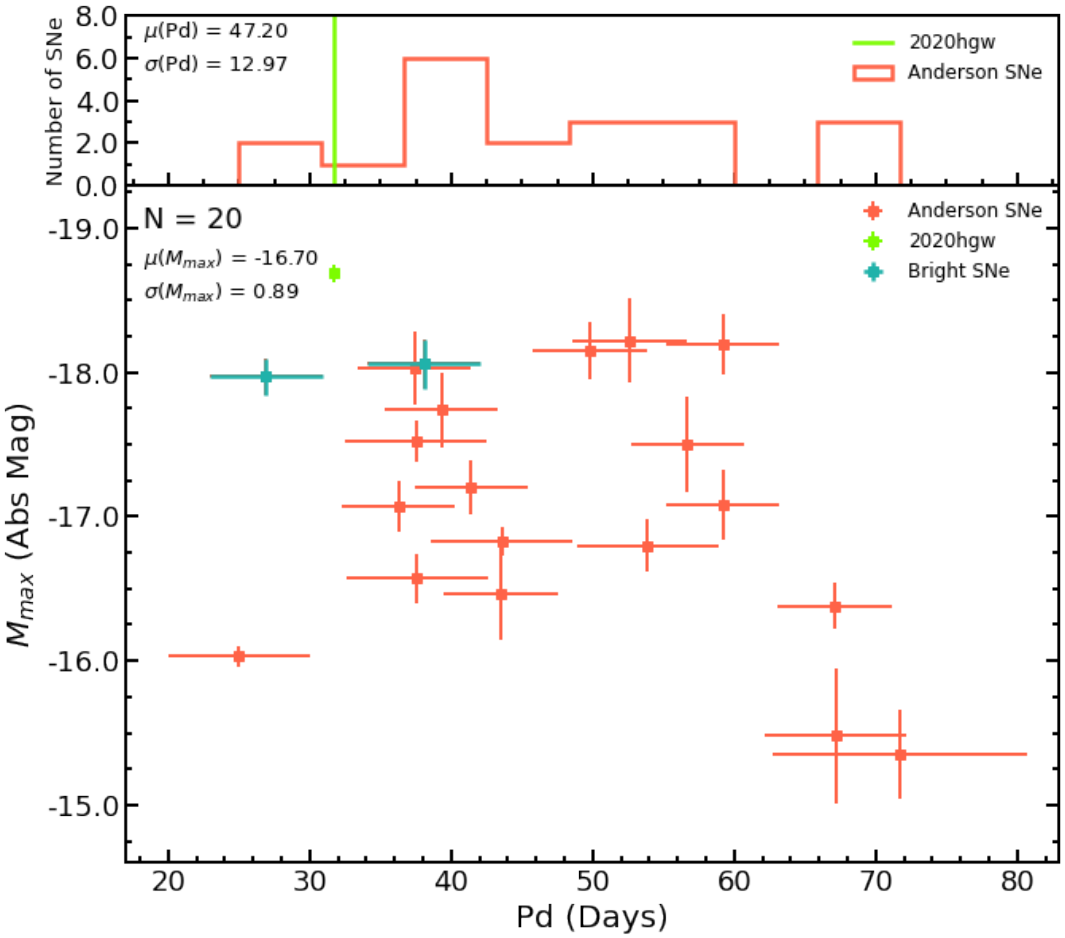

Figure 16: Plateau duration, Pd, versus maximum brightness, M_{max}, for SNe from Anderson et al. 2014, and 2020hgw. SNe from Anderson et al. 2014[9] are marked in red, two remarkably bright SNe from that paper are marked in blue[8], and 2020hgw is marked in green. The histogram at the top shows the distribution of the Anderson et al. 2014[9] SNe for plateau duration, with a green line marking where 2020hgw lies in this distribution at 1.19 σ away from the mean.

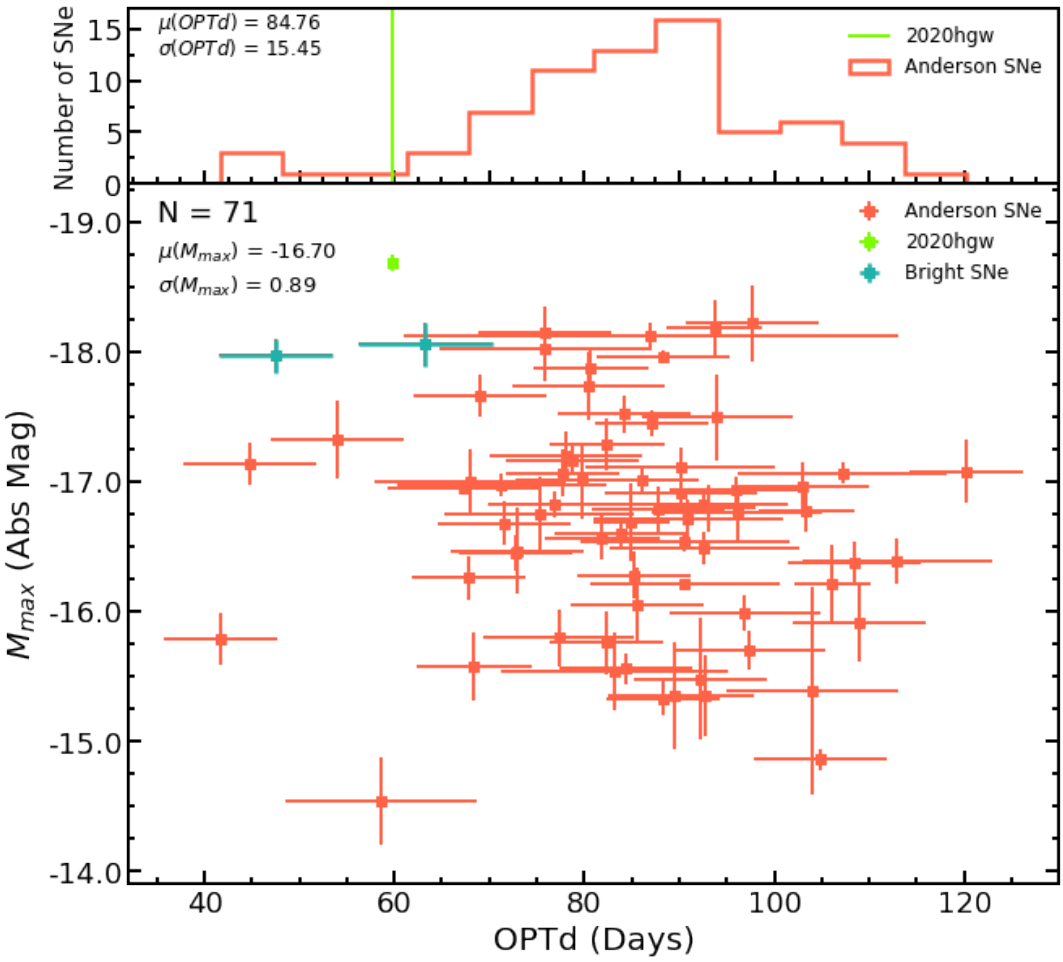

Figure 17: Optically thick phase duration, OPTd, versus maximum brightness, M_{max}, for SNe from Anderson et al. 2014, and 2020hgw. SNe from Anderson et al. 2014 are marked in red, two remarkably bright SNe from that paper are marked in blue[8], and 2020hgw is marked in green. The histogram at the top shows the distribution of the Anderson et al. 2014 SNe for optically thick phase duration, with a green line marking where 2020hgw lies in this distribution at 2.04 σ from the mean.

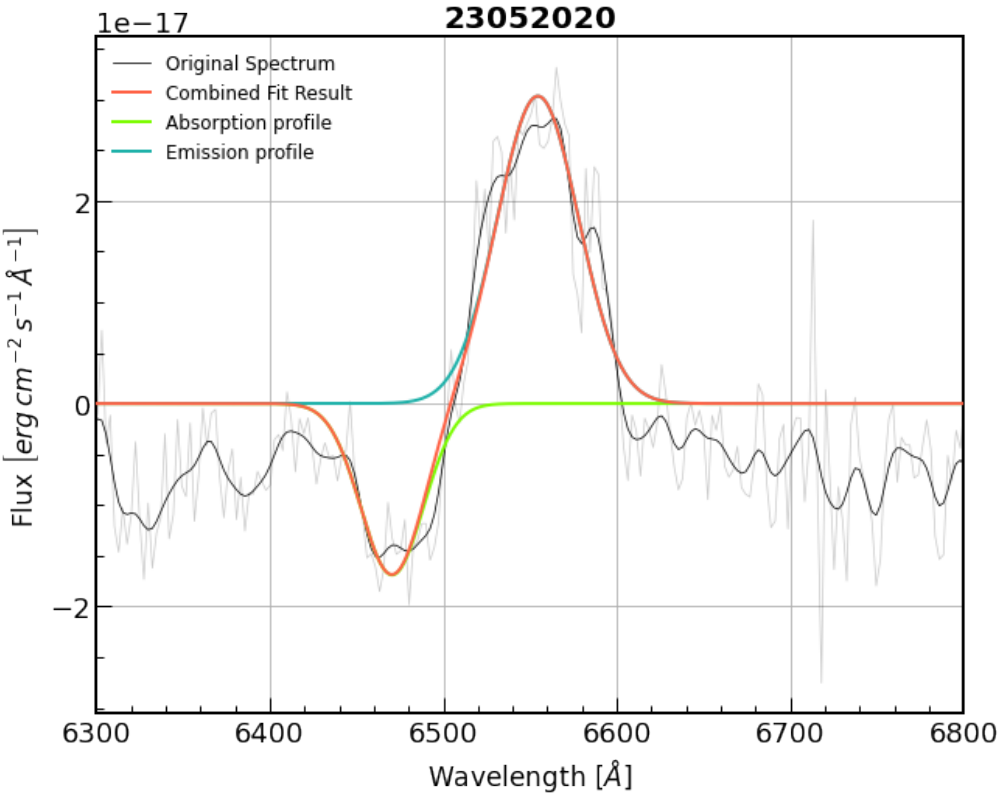

Figure 18: Fit to H_α absorption and emission line for the spectrum taken on May 23rd 2020. The Green line presents the absorption profile fit, the blue line presents the emission profile fit and the red line shows the combined fit. The black line presents the original, flattened spectrum.

In Figures 18-21 a cut around the H_α line is shown for the [2305]2020, [2805]2020, [0906]2020 and [1907]2020 spectra, with fits to the H_α absorption and H_α emission shown in green and blue respectively.

Fits of the spectra are used to determine the velocity of the H_α line for both emission and absorption. They were also used to find the absorption over emission(a/e) coefficients so we can see their evolution over time, and to compare them with the SNe from Anderson et al. 2014 and Gutiérrez et al. 2014. In Table 1 the measured H_α emission and absorption velocities, along with a/e coefficients can be seen.

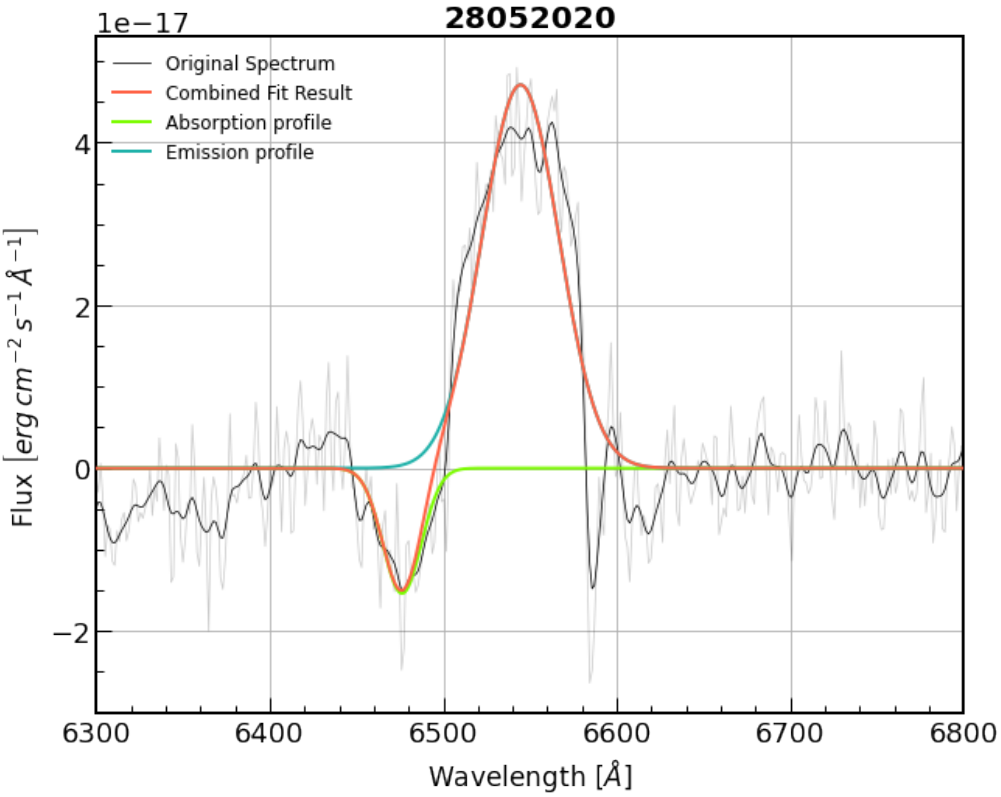

Figure 19: Fit to H_α absorption and emission line for the spectrum taken on May 28th 2020.The Green line presents the absorption profile fit, the blue line presents the emission profile fit and the red line shows the combined fit. The black line presents the original, flattened spectrum.

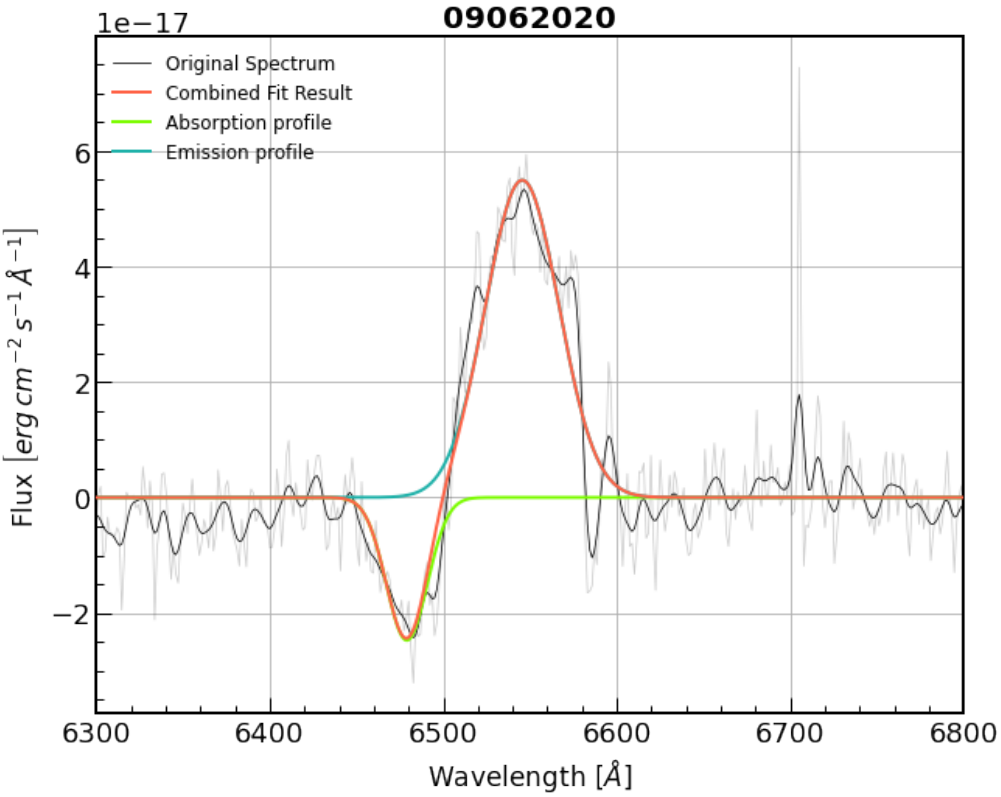

Figure 20: Fit to H_α absorption and emission line for the spectrum taken on June 9th 2020.The Green line presents the absorption profile fit, the blue line presents the emission profile fit and the red line shows the combined fit. The black line presents the original, flattened spectrum.

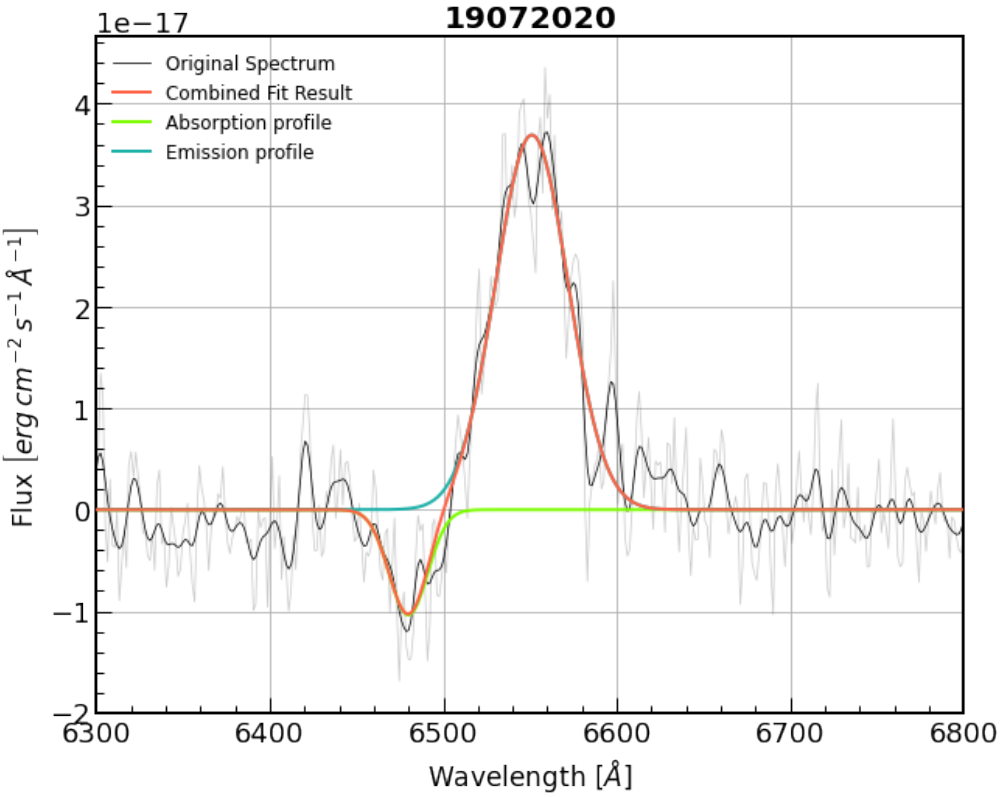

Figure 21: Fit to H_α absorption and emission line for the spectrum taken on July 19th 2020.The Green line presents the absorption profile fit, the blue line presents the emission profile fit and the red line shows the combined fit. The black line presents the original, flattened spectrum.

Spectrum	H_α em. vel. [km/s]	H_α abs. vel. [km/s]	a/e coeff.
[2305]2020	473.34 ± 1.68	4314.11 ± 12.03	0.4321 ±0.0003
[2805]2020	930.24 ± 3.13	4051.33 ± 6.93	0.16444 ±0.00013
[0906]2020	886.33 ± 2.86	3926.01 ± 7.15	0.2519 ±0.0002
[1907]2020	632.72 ± 2.02	3884.18 ± 6.65	0.14977 ±0.00012

Table 1: Table showing the measured properties of the H_α P-Cygni profile: the emission and absorption velocity and a/e coefficient at the four epochs from 2305 to 1907.

4.7 Gutiérrez et al. 2014 and their SNe

In Figure 22 the H_α a/e is plotted versus the H_α emission velocities. The a/e coefficients for 2020hgw is within the population from Gutiérrez et al. 2014[21] lying 0.49, 1.06, 0.59 and 1.14 σ away from the mean of the sample. However, the H_α emission velocities at the successive epochs are 1.56, 1.74, 1.83 and 1.87 σ away from the mean, and as seen in Figure 22, just on the edge of the general population. In Gutiérrez et al. 2014 though, they state that they measure the spectral properties for the spectra at the time in closest proximity to $t_{tran}+10$ days, so at the start of the recombination phase. For 2020hgw: $t_{tran}+10 = 27.60$, making the closest spectrum the [2305]2020 spectrum. This is also the spectrum for which the H_α emission velocities and a/e coefficient are closest to the mean of the sample population at 1.56 and 0.49 σ away respectively.
In the discussion I will get into the possible implications of this.

In Figure 23 the H_α a/e coefficient versus M_{max} is plotted, with the Gutiérrez et al. 2014 SNe and the 2020hgw values. 2020hgw is clearly the brightest of these SNe, but also not far off from the rest of the population at 1.89 σ away from the mean. As above, the a/e coefficient for [2305]2020 is approximately in the middle of the population.

In Figure 24 the duration of the optical thickness is plotted against the H_α a/e coefficient. 2020hgw is on the edge of the population in both respects, but once again within the general scatter of the population. It is however, on the very short end of the duration of the optically thick phase, just as with the plateau duration. So there is not just a wide peak and long first decline to make up for a shorter plateau.

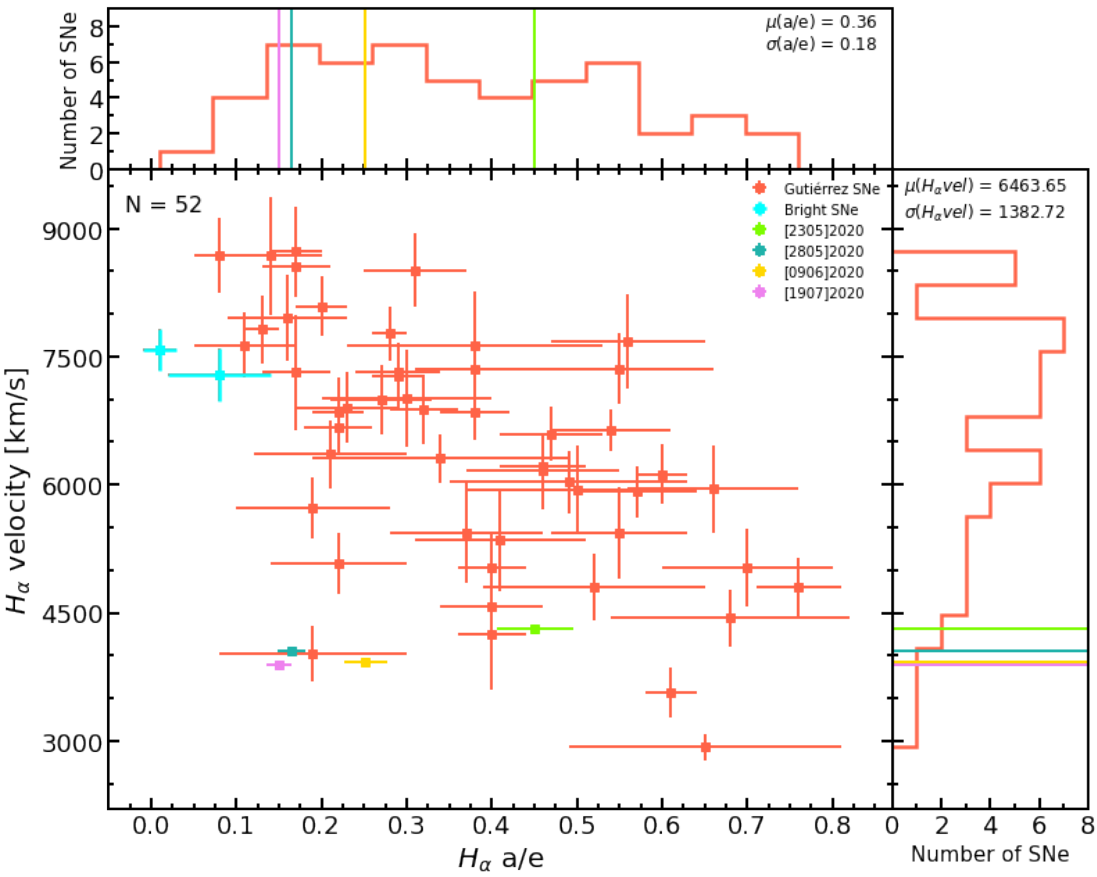

Figure 22: H_α a/e coefficient versus H_α emission velocities for the Gutiérrez et al. 2014[21] SNe, and for 2020hgw for the four different dates on which spectra were taken i green, blue, yellow and purple, and the two bright SNe 2006Y and 2006ai in cyan[8]. On the histograms are shown the distributions of the Gutiérrez SNe with lines representing the four dates of 2020hgw.

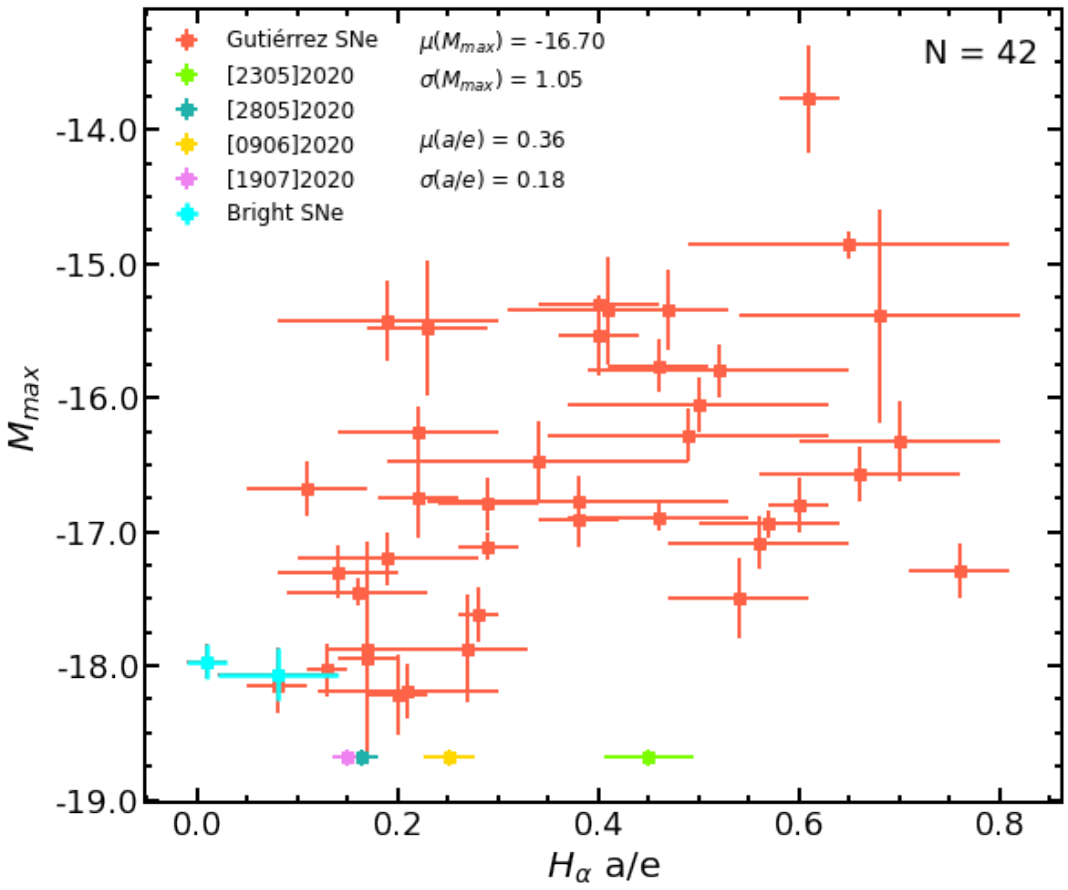

Figure 23: H_α emission velocities versus M_{max} is plotted, with the Gutiérrez et al. 2014 SNe in orange, the four different values for 2020hgw in green, blue, yellow and purple, and the two bright SNe 2006Y and 2006ai in cyan[8]. The uncertainty on M_{max} for 2020hgw is so small it is not visible, though it is there.

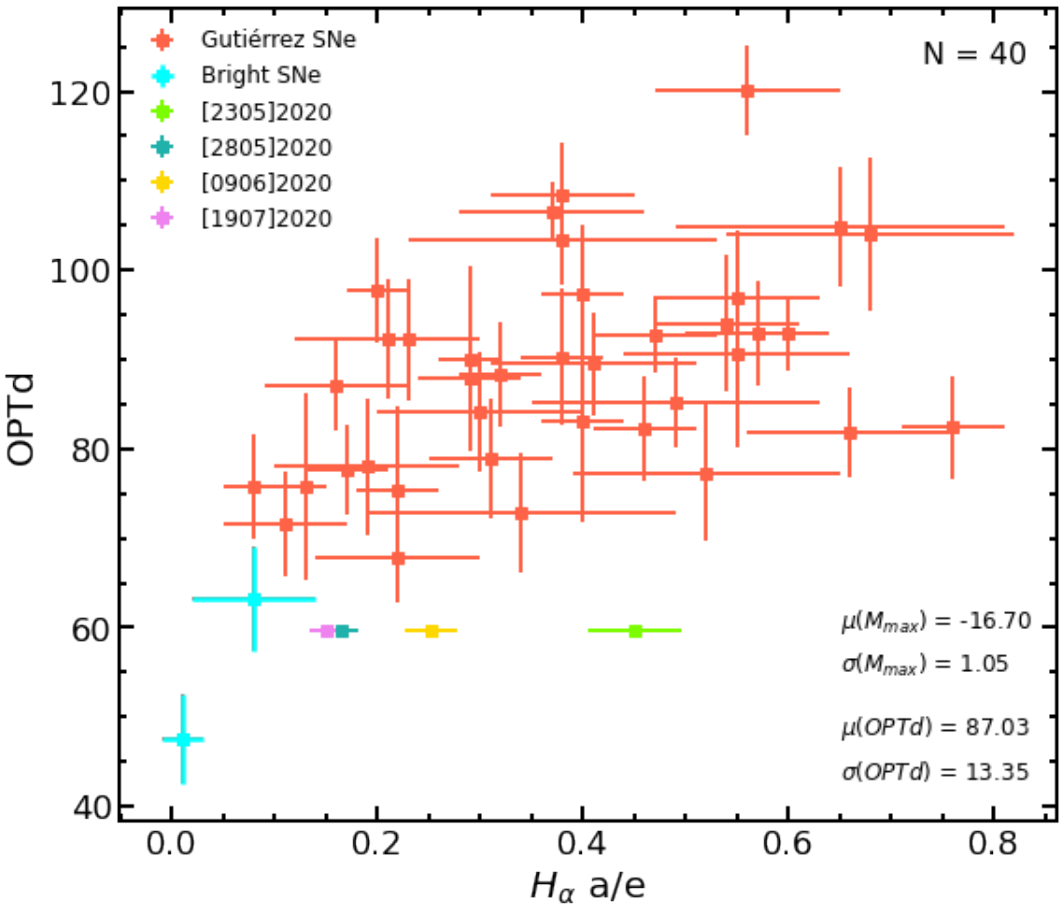

Figure 24: H_α a/e coefficient versus OPTd, with the Gutiérrez et al. 2014[21] SNe in orange, the four dates for 2020hgw in green, blue, yellow and purple, and two bright SNe, 2006Y and 2006ai, in cyan[8]

.

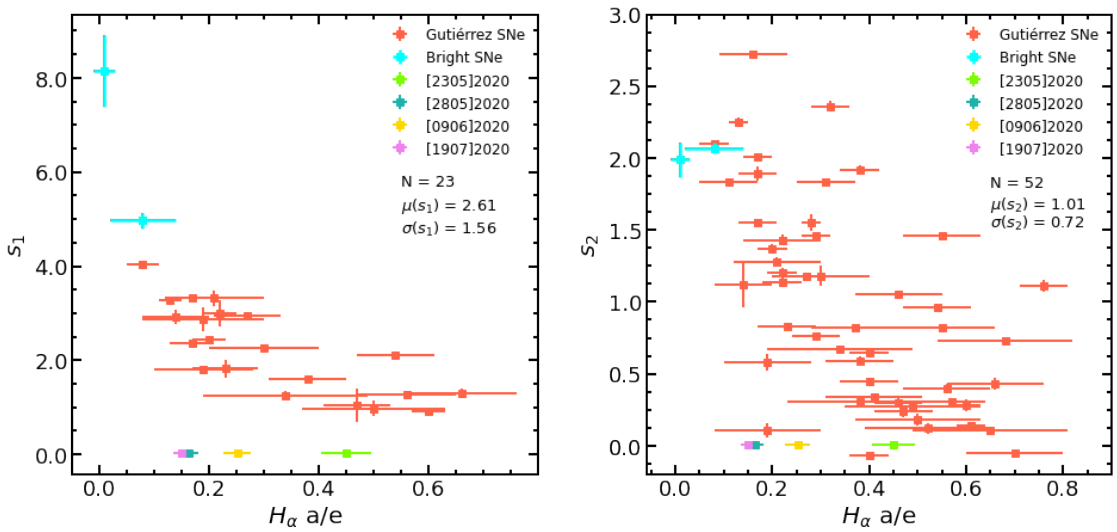

Figure 25: In the figure on the left s_1 versus H_α is plotted with the Gutiérrez et al. 2014 SNe in orange, and the four different values for 2020hgw in green, blue, red and purple. In the figure on the right s_2 versus H_α is plotted with the Gutiérrez et al. 2014 SNe in orange, and the four different values for 2020hgw in green, blue, yellow and purple. In both figures are marked 'Bright SNe', these are 2006Y and 2006ai.[8]

In Figure 25 the Gutiérrez et al. 2014[21] population is shown with s_1 and s_2 versus H_α a/e with 2020hgw values for the different dates of the spectra. For both s_1 and s_2 2020hgw lies at the lowest end of the Gutiérrez et al. 2014 population. It lies 1.66 and 1.39 σ away from the mean for s_1 and s_2 respectively. And so statistically not far away though it almost looks like it.

4.8 The Bolometric Lightcurve

With `superbol` using the g-ZTF, r-ZTF, i, c and o filter data, I obtained fits resulting in a bolometric luminosity light curve. By integrating under this I calculated the total radiated energy. It was found to be: $1.559 \pm 0.004 \cdot 10^{44} erg\, s^{-1}$. The obtained bolometric light curve is seen in Figure 26 where the red points present the observed flux, and the green points present the observed flux plus a black body correction for regions outside the observed data range.

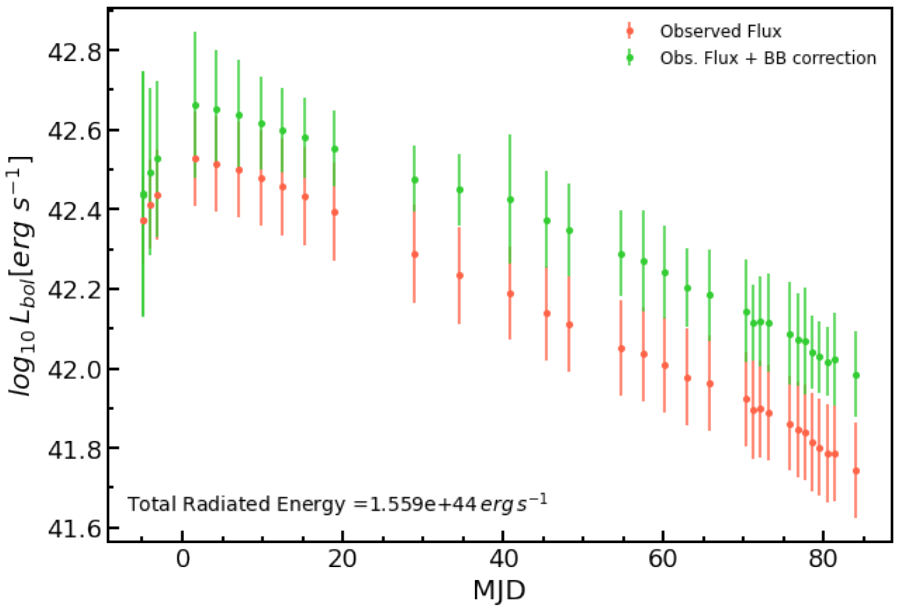

Figure 26: Bolometric light curve obtained with superbol. Presented in red is the observed flux, and in green is the observed flux plus a blackbody correction.

5 Discussion

2020hgw is a very bright Type IIP SN with its peak absolute magnitude of -18.69 ± 0.065. It is also one of the shortest measured plateau length to date at 31.70 ± 0.64 days. I will even argue that the plateau is probably shorter than this, as this length is found by t_{end} - t_{tran}, but because these are found analytically they don't seem entirely accurate visually. Looking at Figure 14 t_{tran} should be about four days later at 22 days post peak, and t_{end} about five days earlier at 44 days post peak, putting the plateau duration at only 25 days. This would in Figure 16 put 2020hgw on line with the two shortest plateau lengths of the Anderson SNe.

One might question the validity of the results and comparisons of 2020hgw with the other samples as a lot of their analysis is done for V-band observations and the analysis of 2020hgw is done for r-ZTF. And to support that, in Figure 27 the transmission for the V-band filter used by the CSP[22]. However, given the recessional velocities, and thereby the redshift, of the Anderson et al. 2014 sample, the mean wavelength that is probed for the Anderson et al. 2014 sample is much closer to the

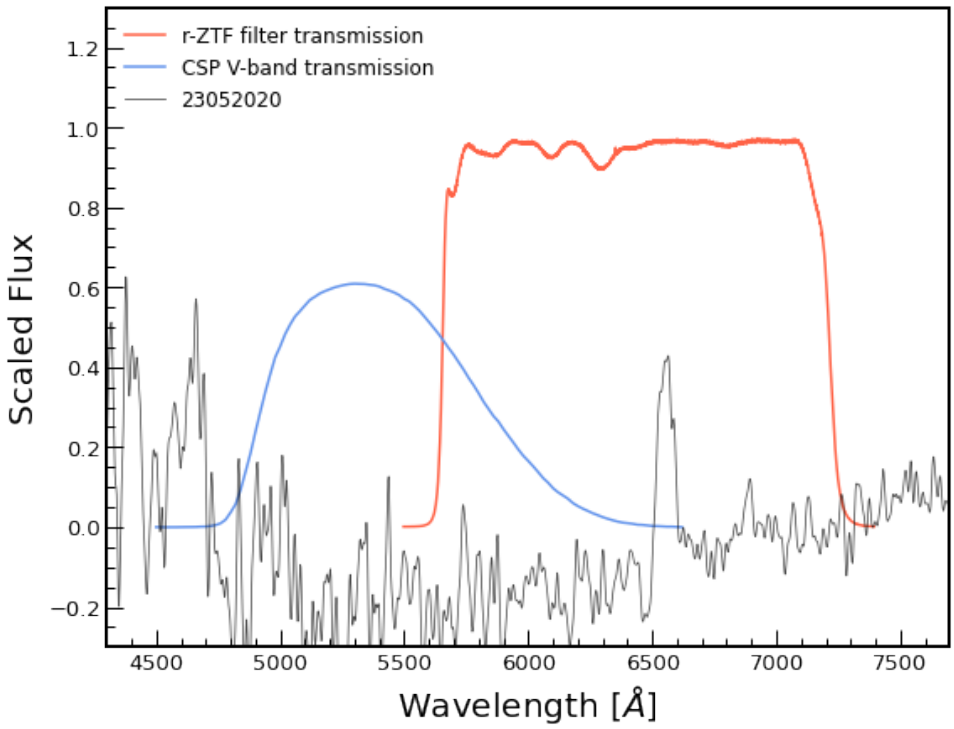

Figure 27: Filter transmission for a standard V-band filter presented in blue and for the r-ZTF filter presented in red.

effective wavelength of the r-ZTF band than the g-ZTF band given the redshift of 2020hgw. I will therefore argue that using the r-ZTF data for 2020hgw makes the data more comparable to the V-band data of their sample, than bluer filters would.

The values obtained from the light curve fit with Equation 19 have to be treated with caution. Though there is also an example in the original paper where they use the Gaussian to fit the light curve peak, most of them are fit with the Gaussian accounting for the curvature of the plateau. This is mainly due to a lack of early data for the SNe in the paper, but it also means that the model was built more with that configuration in mind, and with the expectation of fitting it like that. For 2020hgw it did not make sense to fit the Gaussian to the plateau, but rather to the peak as there were many more early data points. This should not have a large effect on the important fit values, given that they also apply it like this in some cases, but it means that we have to take this into consideration when comparing the fit values to those of the other SNe.

From the comparison plots and general data on SNe II, we know that 2020hgw with its peak magnitude just shy of -19, is a very bright SN in comparison with other Type II SNe, where the brighter ones typically have peak luminosities of $M \sim -17$ to -18. With this we can infer that there must be some interaction with an envelope surrounding the SN, as interaction will increase the luminosity of a such event. Normally interaction will mean that there is shock ionising of a surrounding shell, which we also see evidence of for 2020hgw with the plateau as this comes from the shell getting ionised by the initial shock waves and then cooling.

Gutiérrez et al. 2014[21] find that for the general Type II SN population there is a strong correlation between having a smaller a/e coefficient, higher s_1 and s_2, high luminosity and short optically thick phase duration. For 2020hgw with its high luminosity and short optically thick phase duration, this does not quite fit, as it has very low values for both s_1 and s_2 at 0.024 ± 0.006 and 0.011 ± 0.005, whereas the other two bright SNe have s_1 values around 5.0 and 8.0, and s_2 values around 2.0 making them fit this correlation better.
Whether this is the result of 2020hgw interacting with the surroundings, or it highlights a broader spread in s_1 and s_2 values than what we have previously seen, is unclear.

Additionally as stated in Gutiérrez et al. 2014[21] there has been found to be a correlation between larger a/e coefficients for Type IIPs than Type IILs. For 2020hgw it initially lies around the centre of the distribution of the Gutiérrez et al. 2014 SNe, and as it develops, the coefficient gets smaller. Again, in the paper they measure the coefficients for the spectrum in closest time proximity to t_{tran} + 10 days which for 2020hgw is May 23rd. This spectrum has an $a/e = 0.4321 \pm 0.0003$, even lying on the higher side of the mean putting it alongside typical IIPs, but quite far off from the other bright SNe[8],[9]. However, for 2020hgw the a/e weakens at the later epochs, which in other Type II SNe has been attributed as a signature of interaction as this 'fills in' the absorption component.

From the spectra I was able to calculate the H_α velocities right at the start of the plateau, at the middle of the plateau and at the end of the plateau as can be seen in Figure 8. These velocities give us a picture of how the ejecta is clearly slowing down: in just five days the absorption velocity slows from 4314.11 ± 12.03 km/s to

4051.33 ± 6.93 km/s, during the beginning of the plateau. By the end of the plateau, just twelve days later, the emission velocity has dropped to 3926 ± 7.15 km/s.
The fact that the velocities drop so clearly tells us roughly when the ejecta pushed out from the explosion, collides with the surrounding envelope. The large amount that the velocities drop with also tells us that the envelope has to be quite dense, otherwise that gradient would be much smaller.
The shell would also have to be very dense to explain the lower H_α velocities to begin with, which is in contrast to what Gutiérrez et al. 2014 find; that the brighter SNe usually have low a/e and high H_α velocities.

Further support for the shell being dense comes from the width of the emission and absorption lines. Usually the broad lines of a Type IIP come from fast moving ejecta, but even though 2020hgw does not lie far outside the general population at 1.56 σ away from the mean, it is still clear from looking at Figure 22 that it lies at the lower end and on the edge of the population. The lines therefore appear somewhat narrower than for a typical Type IIP SN.
An important thing to note here is also that not only are the velocities at the lower end of the general population, they are much lower than those of the bright SNe as seen in Figure 22.
In Gutiérrez et al. 2014[21] they also mention that Type IIL SNe typically have narrower P-Cygni profiles than IIPs, and with 2020hgw having a short plateau and a narrower P-Cygni profile, this could suggest bridging between the two types.

We also see none of the narrow emission that would come from the ejecta shocking a colder, further out shell that would also be much denser, giving the shorter mean free path for the photons that provide the narrow lines of a IIn. 2020hgw therefore does not exhibit the features of a typical typical Type IIn.

We only see the low-end high velocity lines, which would appear as the result of the ejecta interacting with either a dense, clumpy wind or from the dense shell having been quickly shocked and thereby ionised, allowing for a longer free path for the photons. Either way, the emission is most likely to come from something very dense but thin, surrounding the SN. They also mention in Gutiérrez et al. 2014[21] that it has previously, though on a small set of Type II SNe, been found that low luminosity SNe have narrow P-Cygni profiles, which is the opposite of the case for 2020hgw. It

is very luminous and yet still has narrower spectral lines.

In Figure 16 there also seems to be a correlation between luminosity and plateau length - the brighter the SN, the shorter the plateau, as marked by the SNe 2006Y and 2006ai, which were in the paper[9] marked as especially bright SNe. Additionally, in Gutiérrez et al. 2014 they also find that the brighter SNe have shorter optically thick phase durations, which is also true for 2020hgw, with only one of the Gutiérrez et al. 2014 SNe having a smaller OPTd value and 2020hgw being brighter than all of their SNe.
This relatively short plateau duration, can possibly be explained by this temper tantrum. Shortly before dying the star might be hydrostatically unstable, leading it to have minor expansions and reductions in size sometimes leading to the star throwing off a lot of its outer material. This could cause it to leave behind only a very narrow and dense shell of material, lying very close to the star. This explanation would also account for the relatively large drop in emission and absorption velocities at the beginning of and throughout the plateau with a very dense shell being able to halt the final shock wave.

If we were to say something about the progenitor, it is likely that it had a period of significant mass loss as has been shown to happen for RSGs, the progenitors of Type IIPs. Possibly a first wave of mass loss some time before the SN occurred, and then a last temper tantrum of mass loss right before the actual SN, leaving a close-by, thin and very dense shell.

One plausible explanation that this SN seems so unique with the short duration of the plateau and bright peak, likely comes down to the historically low cadence of observations of SNe - and lack of knowledge on how to find them before they explode. This would mean that if a SN only had a plateau of 10-40 days, and an average observational cadence of 7-10 days, it would have been easy to miss a short plateau and put the possibly single data point down to an outlier to be discarded. This is why the Young Supernova Experiment with their 2-3 day observational cadence is a great addition to the field of SN research and why we are now likely to find more short-plateaued SNe in the future, as there is growing evidence that they do exist.

6 Conclusion

I have statistically, in addition to visually, tested that fitting the light curve with two separate lines for the post-peak decline and the plateau, gives a better result than fitting with one combined line. We can from this conclude that 2020hgw can be described as a Type IIP SN, and not a IIL. I also conclude that the plateau is clearly visible in two of the five filters analysed, though in one filter this is only found by visual inspection and not measured at this point.

From fitting to the light curve in the r-ZTF band I find the middle of the transition to the radioactive tail to be at $t_{PT} = 64.76 \pm 5.66$. From t_{PT}, according to the methods of Anderson et al. 2014[9], I find the time of transition from post-peak decline to plateau to be at $t_{tran} = 17.60 \pm 0.47$ days and the end of the plateau to be at $t_{end} = 49.30 \pm 0.44$ days.
From these I then find the duration of the plateau to be $Pd = 31.70 \pm 0.64$, and the duration of the optically thick phase to be $OPTd = 59.79 \pm 0.44$ days.
These values for Pd and $OPTd$ put 2020hgw on the map as one of the shortest plateau durations measured yet with only two of the Anderson et al. 2014[9] having slightly shorter Pd.

From comparing to two other samples of Type IIP SNe, I can also conclude that 2020hgw is, with its peak magnitude of -18.69 ± 0.065 in r-ZTF, a very bright Type IIP SN.
I also find that 2020hgw exhibits somewhat slow expansion velocities despite previous papers finding an opposite correlation between luminosity and expansion velocities and 2020hgw is visibly on the edge of the rest of the population with slower velocities, and much slower velocities than the two SNe that have been cited as remarkably bright[8].
These features can according to theory, be interpreted as interaction of the SN with ejected material.

Whether 2020hgw is a typical example of a 'short plateau SN' or if it is an exceptional case, remains unclear. In the future, with possible observations of more 'short plateau IIPs', it should become clearer.

7 Acknowledgments

First of all I would like to thank my supervisor Charlotte for her endless support, patience, understanding and wonderful presence. Not at any point was I afraid of asking stupid questions or being honest about being exhausted and for this I am so grateful, it really has been wonderful. And thank you for the unending enthusiasm for my pretty plots, I believe this enthusiasm is what drove me most of the way.

I would also like to thank Cecilie for sending me Charlotte's way while I was looking for a supervisor.

I also want to thank Kasper for his patience with me during the final month, and for cooking for me and making sure I drank water. I am sure I would have perished without his help.

This research has made use of the Spanish Virtual Observatory (`https://svo.cab.inta-csic.es`) project funded by MCIN/AEI/10.13039/501100011033/ through grant PID2020-112949GB-I00.[23][24]

The data presented here were obtained [in part] with ALFOSC, which is provided by the Instituto de Astrofisica de Andalucia (IAA) under a joint agreement with the University of Copenhagen and NOT.

References

[1] *Supernova*. Oct. 2022. URL: `https://en.wikipedia.org/wiki/Supernova`.

[2] *CNO cycle*. Sept. 2022. URL: `https://en.wikipedia.org/wiki/CNO_cycle`.

[3] Jason Kendall. *Core-Collapse Supernovae*. Sept. 2018. URL: `https://youtu.be/rdgOkSKPP1Y`.

[4] Terry A. Matilsky. *Analyzing the Universe - Course Wiki: The Sky is Falling!* 2014. URL: `https://www.physics.rutgers.edu/analyze/wiki/cc_supernovae.html`.

[5] Swinburne University. *Supernova Classification*. URL: `https://astronomy.swin.edu.au/cosmos/S/Supernova+Classification`.

[6] L. Martinez et al. "Progenitor properties of type II supernovae: fitting to hydrodynamical models using Markov chain Monte Carlo methods". In: *Astronomy & Astrophysics* 642 (Oct. 2020), A143. DOI: 10.1051/0004-6361/202038393. URL: https://www.aanda.org/articles/aa/full_html/2020/10/aa38393-20/aa38393-20.html.

[7] B. Davies. "Red supergiants as supernova progenitors". In: *Philosophical Transactions of the Royal Society A: Mathematical, Physical and Engineering Sciences* 375 (Oct. 2017).

[8] Daichi Hiramatsu et al. "Luminous Type II Short-Plateau Supernovae 2006Y, 2006ai, and 2016egz: A Transitional Class from Stripped Massive Red Supergiants". In: *Astrophysical Journal* 913.1 (May 2021), p. 55.

[9] Joseph P. Anderson et al. "Characterizing the V-band Light-curves of Hydrogen-rich Type II Supernovae". In: *The Astrophysical Journal* 786.1, 67 (May 2014), p. 67. URL: https://ui.adsabs.harvard.edu/abs/2014ApJ...786...67A.

[10] *Red supergiant*. Oct. 2022. URL: https://en.wikipedia.org/wiki/Red_supergiant.

[11] Eli Kasai. Apr. 2013. URL: https://www.researchgate.net/figure/a-Example-of-a-P-cygni-profile-showing-a-broad-emission-line-peak-and-an-absorption_fig10_282018418.

[12] Matthew J. Graham et al. "The Zwicky Transient Facility: Science Objectives". In: *Publications of the Astronomical Society of the Pacific* 131.1001 (May 2019), p. 078001. DOI: 10.1088/1538-3873/ab006c. URL: https://doi.org/10.1088/1538-3873/ab006c.

[13] D. O. Jones et al. "The Young Supernova Experiment: Survey Goals, Overview, and Operations". In: *The Astrophysical Journal* 908.2, 143 (Feb. 2021), p. 143. DOI: 10.3847/1538-4357/abd7f5.

[14] Armin Rest and Rick White. *PS1 Filter properties*. Dec. 2017. URL: https://outerspace.stsci.edu/display/PANSTARRS/PS1+Filter+properties#PS1Filterproperties-Filterdescriptions.

[15] J. L. Tonry et al. “ATLAS: A High-cadence All-sky Survey System”. In: *Publications of the Astronomical Society of the Pacific* 130.988 (June 2018), p. 064505.

[16] *Swift's Ultraviolet/Optical Telescope(UVOT)*. URL: https://swift.gsfc.nasa.gov/about_swift/uvot_desc.html.

[17] Support Astronomers. *User's Guide to the Kast Double Spectrograph: Red Side*. Mar. 2021. URL: https://mthamilton.ucolick.org/techdocs/instruments/kast/hw_red.html.

[18] Matt Nicholl. *Superbol*. 2018. URL: https://github.com/mnicholl/superbol.

[19] Felipe Olivares E. et al. “THE STANDARDIZED CANDLE METHOD FOR TYPE II PLATEAU SUPERNOVAE”. In: *The Astrophysical Journal* 715.2 (2010), pp. 833–853. URL: https://doi.org/10.1088/0004-637x/715/2/833.

[20] *How to estimate uncertainty of measurements of equivalent widths*. Jan. 2019. URL: https://astronomy.stackexchange.com/questions/29357/how-to-estimate-uncertainty-of-measurements-of-equivalent-widths.

[21] Claudia P. Gutiérrez et al. “H_α Spectral Diversity of Type II Supernovae: Correlations with Photometric Properties”. In: *The Astrophysical Journal Letters* 786.2, L15 (May 2014), p. L15. DOI: 10.1088/2041-8205/786/2/L15. URL: https://ui.adsabs.harvard.edu/abs/2014ApJ...786L..15G.

[22] July 2021. URL: http://svo2.cab.inta-csic.es/svo/theory/fps/index.php?id=LCO/CSP.V_LC3009&&mode=browse&gname=LCO&gname2=CSP#filter.

[23] Carlos Rodrigo, Enrique Solano, and Amelia Bayo. *SVO Filter Profile Service Version 1.0*. IVOA Working Draft 15 October 2012. Oct. 2012. DOI: 10.5479/ADS/bib/2012ivoa.rept.1015R.

[24] C. Rodrigo and E. Solano. “The SVO Filter Profile Service”. In: *XIV.0 Scientific Meeting (virtual) of the Spanish Astronomical Society*. July 2020, 182, p. 182.